

Supplemental Data

Digital Signaling and Hysteresis

Characterize Ras Activation

in Lymphoid Cells

Jayajit Das, Mary Ho, Julie Zikherman, Christopher Govern, Ming Yang, Arthur Weiss, Arup K. Chakraborty, and Jeroen P. Roose

Index	Page
Section I. Ras-SOS Minimal Model	4
Fig. S1. Schematic representation of the simulation box.	5
Table S1: Rate constants used for Fig. 1b	6
Table S2: Measured or estimated values of concentrations in literature for other cells.	8
Table S3: Parameter Sensitivity of the Minimal Model	9
Fig. S2. Effects of variations of parameters in Fig. 1c	16
Fig. S3. Effects of variations of parameters in Fig. 1c	18
Fig. S4. Effects of variations of concentrations in Fig. 1c	19
Section II. Stochastic Simulation of the Network in Figure 2a	20
Table S4: Reactions and Rate constants for SOS _{cat} transfection simulations	21
Table S5: Concentrations used for SOS _{cat} transfection simulations	21
Table S6: Parameter sensitivity for SOS _{cat} transfections simulations: rate constants measured for related molecules or unknown	22
Table S7: Parameter sensitivity for concentrations used for SOS _{cat} transfection simulations	33
Table S8: Parameter sensitivity for SOS _{cat} transfections simulations: rate constants measured for the pertinent molecules	36
Fig. S5. Effect of change in the binding (k_2) and unbinding (k_{-2}) rates of RasGTP to the allosteric site of SOS _{cat}	43
Fig. S6. Effect of change in the binding rate (k_7) of Rasgrp1 to DAG	44
Fig. S7. Effect of variation of Ras concentration	44
Fig. S8. Effect of variation of Ras-GAP concentration	45
Fig. S9. Effect of variation of rate (k_2) of Ras-GTP binding to the allosteric site of SOS _{cat}	45
Fig. S10. Effect of variation of the binding rate (k_3) of Ras-GDP to the catalytic pocket of SOS _{cat} when the allosteric site of SOS _{cat} is occupied by Ras-GTP	46
Fig. S11. Effect of variation of catalytic rate (k_3^{cat}) of SOS _{cat} when the	

	allosteric site of SOS_{cat} is occupied by Ras-GTP	47
Fig. S12.	Effect of variation of catalytic rate (k_4^{cat}) of SOS_{cat} when the allosteric site of SOS_{cat} is occupied by Ras-GDP	48
Section III. Simulations of Receptor Stimulation		49
Table S9:	Reactions and Rate constants for receptor stimulation simulations	49
Table S10:	Concentrations used for receptor stimulation simulations	51
Table S11:	Measured or estimated values of concentrations in literature for other cells.	52
Table S12:	Parameter Sensitivity for the Rate constants for receptor stimulation simulations	53
Table S13:	Parameter Sensitivity for the concentrations used for receptor stimulation simulations	60
Fig. S13.	Variation of TCR-pMHC binding rate (k_{10})	62
Fig. S14.	Variation of LAT unbinding rate (k_{-16}) from pZAP-LAT complexes	63
Fig. S15.	Variation of PLC γ unbinding rate (k_{-19}) from PLC γ -pLAT complexes	64
Fig. S16.	Variation of DAG production rate (k_{22}^f)	65
Fig. S17.	Variation of unbinding rate (k_{-26}) of SOS from Grb2 rate	66
Fig. S18.	Variation in ZAP70 concentration	67
Fig. S19.	Variation in LAT concentration	67
Fig. S20.	Variation in Grb2 concentration	68
References		69
Section IV. Cell biological procedures		70
	Cell lines, stimulations, inhibitors, plasmids, and transfections	70
	Western blot analysis	70
	Intracellular FACS staining for P-ERK	70
	Ras activation assays	71
Section V. Figures S21-S29		73
Fig. S21	$SOS1_{cat}$ expression in wildtype and RasGRP1 deficient cells	73
Fig. S22	RasGRP1 deficiency results in a relative block	74
Fig. S23	Priming of the allosteric pocket in $SOS1_{cat}$ with H-RasG59E38	75
Fig. S24	Digital BCR induced Ras-ERK activation requires SOS	76
	Description of the Hartigan's DIP test	77
Fig. S25	Analog PMA induced Ras-ERK activation requires RasGRP	78
Fig. S26	$SOS1_{cat}$ induces exponential Ras-ERK signals	79
Fig. S27	Kinetics of RasGTP induction in various cell types	80
Fig. S28	ERK phosphorylation patterns of hysteresis experiments	82
Fig. S29	Mathematical model of H-RasG59E38 in RasGRP deficient cells	83
Fig. S30	Trajectories from the stochastic simulation of figure 2B	84

Section VI. Understanding design principles underlying	
bistable Ras activation through minimal models	85
Fig. S31 Minimal model of bistable Ras activation	89

Section I. Ras-SOS Minimal Model

The minimal model is based on the reactions shown in Fig. 1b and is represented by ordinary differential equations described in Materials and Methods of the main text.

The Michealis constants in these equations are defined as,

$K_{3m} = (k_3^{cat} + k_{-3})/k_3$; $K_{4m} = (k_4^{cat} + k_{-4})/k_4$; $K_{5m} = (k_5^{cat} + k_{-5})/k_5$, where, k_n, k_{-n} are the binding, unbinding rates of the substrate (S) to the enzyme (E), respectively, and k_n^{cat} is the rate of production of the product (P) from the complex (ES).

The reaction is shown schematically below:



K_{3m}, K_{4m} and K_{5m} are calculated from Table S1. In many cases, the $K_D (= k_{off}/k_{on})$ values are known for the reactions but the binding (k_{on}) and unbinding (k_{off}) rates are not known. Therefore, we carried out a parameter sensitivity analysis to show the robustness of our results to variations of the parameters upto 10 fold. The details of this analysis are shown in Table S3. In order to calculate the fixed points we set the left hand sides of Eqs. 1a, 1b and 1c in Materials and Methods of main text to zero and evaluate the concentrations from the resulting algebraic equations. The results are shown in Fig. 1c.

The set of equations in Eq.(1) was solved for the geometry below:

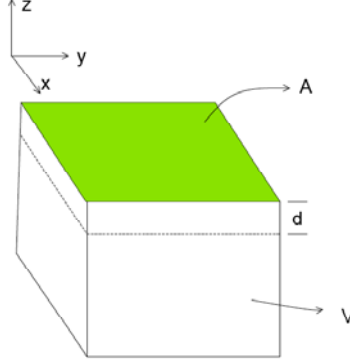


Fig. S1. Schematic representation of the simulation box.

The Ras molecules (R_T and R_D) and the complexes (SR_D , SR_T) that bind to Ras reside in the $z=0$ plane. This is because these molecules are plasma membrane bound. It is assumed that whenever the cytosolic molecules, such as, SOS (S) and Ras-GAPs, come within a small distance (d) of the plasma membrane they interact with the membrane species. We have taken, $d=1.7$ nm, which is the radius of gyration of a Ras molecule (l). Diffusion coefficients of the molecules for which measurements exist are fast enough (2) that the system is well mixed on this length scale. So, we have assumed is well mixed for the other molecular species as well. The signaling events we simulate will occur in several such independent regions adjacent to the cell membrane. One can write the concentrations of the membrane bound molecules in the following way.

$$[R_D(t)] = \frac{N_{R_D}(t)}{Ad} \theta(d+z), \quad [SR_D(t)] = \frac{N_{SR_D}(t)}{Ad} \theta(d+z), \quad [SR_T(t)] = \frac{N_{SR_T}(t)}{Ad} \theta(d+z),$$

where, A is the area of the surface and $\theta(x)$ is the Heaveside step function. $\theta(x) = 1$ for $x \geq 0$ and $\theta(x) = 0$, for $x < 0$. The cytosolic species (S , R_{GAP}) are distributed uniformly in a volume V , and their concentrations can be written as, $[S(t)] = \frac{N_S(t)}{V}$, and $[R_{GAP}(t)] = \frac{N_{R_{GAP}}(t)}{V}$. In our calculations, we take $V=0.08$ (μm)³, and $A=4.0(\mu\text{m})^2$, both these values make sure that the diffusion time of the molecules in the volume V is much faster than the reaction time scales. The parameters are named in the following way: For a reaction labeled,

n. $E + S \xrightleftharpoons[k_{-n}]{k_n} ES \xrightarrow{k_n^{cat}} E + P$, k_n , k_{-n} and k_n^{cat} denote the binding (k_{on} rate), unbinding (k_{off} rate) and the catalytic rates (k_{cat}) respectively for the n th reaction. The rates used in solving the equations in (1) were calculated from the following table:

Table S1: Rate constants used for Fig. 1b

Reaction	k_{on} ((μM) ⁻¹ s^{-1})	k_{off} (s^{-1})	K_D ((μM))	k_{cat} (s^{-1})
1. (allosteric pocket GDP binding-unbinding) $\text{SOS}_{allo} + \text{Ras-GDP} \leftrightarrow \text{SOS}_{allo} - \text{Ras-GDP}$	0.12	3.0	24.5 Ref. (3)	N/A
2. (allosteric pocket GTP binding-unbinding) $\text{SOS}_{allo} + \text{Ras-GTP} \leftrightarrow \text{SOS}_{allo} - \text{Ras-GTP}$	0.11	0.4	3.6 Ref. (3)	N/A
3. (catalytic pocket reaction when the allosteric pocket is occupied with GTP) $\text{SOS}_{allo} - \text{Ras-GTP} + \text{Ras-GDP} \leftrightarrow \text{SOS}_{allo} - \text{Ras-GTP-Ras-GDP} \rightarrow \text{SOS}_{allo} - \text{Ras-GTP} + \text{Ras-GTP}$	0.05	0.1	1.9 Ref. (3)	0.038 Ref. (4)
4. (catalytic pocket reaction when the allosteric pocket is occupied with GDP) $\text{SOS}_{allo} - \text{Ras-GDP} + \text{Ras-GDP} \leftrightarrow \text{SOS}_{allo} - \text{Ras-GDP-Ras-GDP} \rightarrow \text{SOS}_{allo} - \text{Ras-GDP} + \text{Ras-GTP}$	0.07	1.0	14.5 Ref. (3) *	0.003 Ref. (5)
5. (deactivation by RasGAP) $\text{RasGAP} + \text{Ras - GTP} \leftrightarrow \text{RasGAP - Ras - GTP} \rightarrow \text{RasGAP} + \text{Ras - GDP}$	1.74	0.2	0.11 The <i>in-vitro</i> measurements for RasGAPs, such as NF1-333 and GAP-	0.1 Ref. (7, 8) Above value is for the wt p120 RasGAP, value not known

		<p>334 report KD values $\sim 5 \mu\text{M}$ and $\sim 0.1-0.2 \mu\text{M}$ respectively (6), however, these experiments are done in systems saturated with Ras-GAPs which are different from <i>in-vivo</i> conditions.</p> <p>Therefore, we choose a K_D of $\sim 0.1 \mu\text{M}$ and do a parameter sensitivity on this value.</p>	for CAPRI.
--	--	--	------------

* Rate known for Ras binding to the catalytic pocket of SOS when the allosteric pocket is mutated so that the allosteric pocket is inactive. The direct measurement of Ras-GDP binding the catalytic pocket when the allosteric pocket is occupied by Ras-GDP is not reported explicitly, we therefore do a 10 times variation of the on and off rates for our parameter sensitivity analysis and do not find any qualitative change in results.

In our calculation we use molecules/ $(\mu\text{m})^3$ or molecules/ $(\mu\text{m})^2$ as concentration variables, so the rate constants are converted to the appropriate units. The following conversion table may help the reader.

Unit Conversion Table:

$$1\mu\text{M} = 600 \text{ molecules} / (\mu\text{m}^3)$$

$$(k_{\text{on}})_{3\text{D}} = 1 (\mu\text{M})^{-1}\text{s}^{-1} = 0.16 \times 10^{-2} (\mu\text{m})^3/\text{molecules s}^{-1}$$

Concentrations used for Fig. 1b:

We have used a initial Ras-GDP, and Ras-GAP concentrations of 75 molecules/ $(\mu\text{m})^2$, 125 molecules/ $(\mu\text{m})^3$ respectively.

Note none of the concentrations used are known for lymphocytes. However, some concentrations of these species have been measured or estimated (not measured experimentally) in the literature and vary widely between cell types. This is shown in Table S2.

Table S2: Measured or estimated values of concentrations in literature for other cells.

Concentrations measured or estimated in literature					
Species	Ref. (9) (HeLa)	Ref. (10) (PC12)	Ref. (11) (HeLa)	Ref. (12) (estimated)	Ref. (13) (hepatocytes in rats)
SOS		60 mols/ $(\mu\text{m})^3$	59 mols/ $(\mu\text{m})^3$	60 mols/ $(\mu\text{m})^3$	20 mols/ $(\mu\text{m})^3$
Ras*	240 mols/ $(\mu\text{m})^3$	60 mols/ $(\mu\text{m})^3$	960 mols/ $(\mu\text{m})^3$	120 mols/ $(\mu\text{m})^3$	
Ras- GAP		60 mols/ $(\mu\text{m})^3$	11 mols/ $(\mu\text{m})^3$	1.2 mols/ $(\mu\text{m})^3$	

ND=not detected

* It is difficult to calculate the concentration of Ras in plasma membrane from the quoted cytoplasmic concentrations in literature, because it has contributions from both the plasma membrane and the endo-membranes. However, one can get an upper limit on Ras concentration in the plasma membrane by assuming all the Ras in the measured numbers

came from the plasma membrane. For a HeLa cell, the surface area of the cell is $4 \times 3.142 \times (6.45)^2 \text{ } (\mu\text{m})^2 = 522.8 \text{ } (\mu\text{m})^2$ (9). Therefore, the upper limit of a quoted value of [Ras] will be, $[\text{Ras}] \times 940 / 522 \text{ molecules}/(\mu\text{m})^2 = [\text{Ras}] \times 1.8 \text{ molecules}/(\mu\text{m})^2$. Therefore, $[\text{Ras}] = 240 \text{ mols}/(\mu\text{m})^3$ will give a value of $432 \text{ mols}/(\mu\text{m})^2$ as the upper limit of Ras concentration in plasma membrane of a HeLa cell.

We vary the values of the concentrations in Table S3 and demonstrate that there are no qualitative changes in results. Also note, the values of Ras and Ras-GAP concentrations chosen for the base case in our simulations are on the lower and higher sides of the concentrations reported in literature for other cells, respectively. These values used are conservative estimates of these parameters because by going to higher and lower values of Ras and Ras-GAP levels, respectively, the effect of SOS positive feedback becomes stronger as seen in Table S3.

Table S3: Parameter Sensitivity of the Minimal Model

In many cases the $K_D (= k_{\text{off}}/k_{\text{on}})$ values of reactions are known, but the binding and the unbinding rates are not known, for those cases, we vary k_{on} and k_{off} at the same time keeping the K_D fixed. However, in *in-vivo* environment, the values of the rate constants measured *in-vitro* may vary, therefore, we also report the results of variations of those rate constants as well.

Parameter Varied	Nature of Variation	Results
k_1 and k_{-1} (K_D measured <i>in-vitro</i>)	A. Increase k_1 and k_{-1} 10 fold B. Decrease k_1 and k_{-1} 10 fold	No change in qualitative results for both A and B.
k_1	A. Increase 10 times B. Decrease 10 times	A. Unstable region between A and B in Fig. 1c shrinks a little. B. Unstable region between A and B in Fig. 1c expands. Details shown in Fig.

		S2b. Qualitative features unchanged.
k_{-1}	A. 10 times increase B. 10 times decrease	A. Unstable region between A and B in Fig. 1c expands. B. Unstable region between A and B in Fig. 1c shrinks a little. Qualitative features unchanged.
k_2 and k_{-2} (K_D measured <i>in-vitro</i>)	A. 10 times increase. B. 10 times decrease.	No change qualitative results for both A and B.
k_2	A. 10 times increase. B. 10 times decrease.	A. Unstable points between A and B in Fig. 1c shift to the left. The size of the unstable region decreases. Maximum Ras activation increases. B. Unstable points between A and B in Fig. 1c shift to the right. The size of the unstable region increases. Maximum Ras activation decreases. Details in Fig S2c. No qualitative changes.
k_{-2}	A. 10 times increase. B. 10 times decrease.	A. Similar change as in B for the previous change.

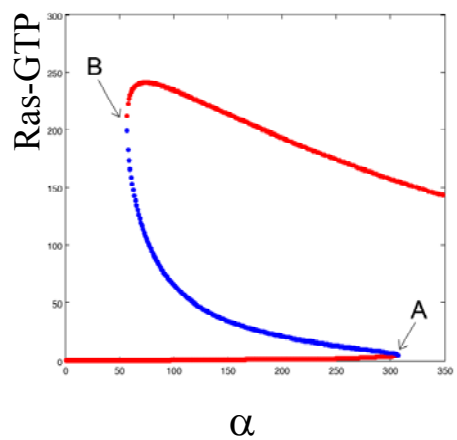
		<p>B. Similar change as in A for the previous change. No qualitative changes.</p>
<p>k_3^{cat}, K_{3m} (k_3^{cat} and K_D measured <i>in-vitro</i>)</p>	<p>A. k_3^{cat} increased 2 times. B. k_3^{cat} decreased 2 times.</p> <p>We vary this parameter by factors of 2 only because we use its value measured <i>in-vitro</i>. By changing it 10 times, the region of bistability will fall in unrealistic values of species concentrations, but the bistability remains.</p>	<p>A. Unstable points between A and B in Fig. 1c undergo a shift to the left and the size of the unstable region decreases. Maximum Ras activation increases.</p> <p>B. Unstable points between A and B in Fig. 1c undergo a shift to the right and the size of the unstable region increases. Maximum Ras activation decreases. Details in Fig. S2d. Qualitative features unchanged.</p>
<p>K_{3m} (k_3^{cat} and K_D measured <i>in-vitro</i>)</p>	<p>A. Increased k_3 and k_{-3} 10 times. B. Decreased k_3 and k_{-3} 10 times. C. Increased k_3 10 times. D. C. Increased k_3 10 times. E. Increased k_{-3} 10 times. F. Decreased k_{-3} 10 times.</p>	<p>A. No change B. No change</p> <p>C. Unstable points between A and B in Fig. 1c shift to the left. The size of the unstable region decreases.</p> <p>D. Unstable points between A and B in Fig. 1c shift to the right. The size of the unstable region increases.</p>

		<p>E. Similar change as in D.</p> <p>F. Similar change as in C.</p> <p>Qualitative features unchanged.</p> <p>Details in Fig. S3a.</p>
k_4^{cat} , K_{4m} (k_4^{cat} measured <i>in-vitro</i>)	<p>A. k_4^{cat} increased 2 times.</p> <p>B. k_4^{cat} decreased 2 times.</p> <p>We vary this parameter by factors of 2 only because we use its value measured <i>in-vitro</i>. By changing it 10 times, the region of bistability will fall in unrealistic values of species concentrations, but the bistability remains.</p>	<p>A. Unstable points between A and B in Fig. 1c undergo a very small shift to the left and the size of the unstable region decreases a little.</p> <p>B. Unstable points between A and B in Fig. 1c undergo a very small shift to the right and the size of the unstable region increases a little. No qualitative changes.</p>
K_{4m} (k_4^{cat} measured <i>in-vitro</i>)	<p>A. Increased k_4 and k_{-4} 10 times.</p> <p>B. Decreased k_4 and k_{-4} 10 times.</p> <p>C. Increased k_4 10 times.</p> <p>D. Decreased k_4 10 times.</p> <p>E. Increased k_{-4} 10 times.</p> <p>F. Decreased k_{-4} 10 times.</p>	<p>A. Unstable points between A and B in Fig. 1c undergo a very small shift to the left.</p> <p>B. Maximum Ras activation decreases a little, and unstable points between A and B in Fig. 1c regions shift to the right. Details in Fig. S3b.</p> <p>C. Unstable points</p>

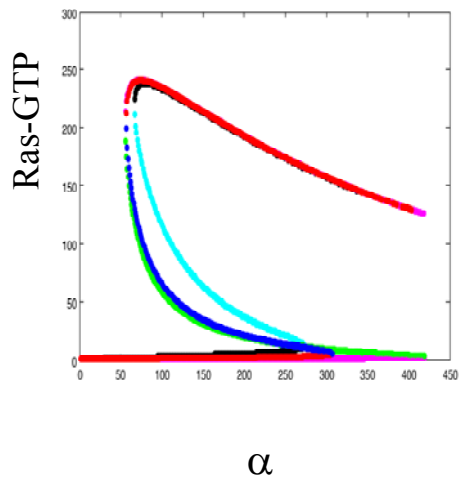
		<p>between A and B in Fig. 1c undergo a very small shift to the left. Details in Fig. S3b.</p> <p>D. The unstable points between A and B in Fig. 1c regions shift to the right, the size of the unstable region expands.</p> <p>E. Similar change as in D.</p> <p>F. Similar change as in D.</p> <p>Qualitative features unchanged.</p>
k_5^{cat}, K_{5m}	<p>A. k_5^{cat} increased 2 times B. k_5^{cat} decreased 2 times</p> <p>We vary this parameter by factors of 2 only because we use its value measured <i>in-vitro</i>. By changing it 10 times, the region of bistability will fall in unrealistic values of species concentrations, but the bistability remains.</p>	<p>A. Unstable points between A and B in Fig. 1c shift to the right. The size of the unstable region increases. Maximum Ras activation decreases.</p> <p>B. Unstable points between A and B in Fig. 1c regions shift to the left. The size of the unstable region decreases and maximum Ras activation increases.</p> <p>Details in Fig. S3c.</p>

		No qualitative changes.
K_{5m}	<p>A. Increase k_5 10 times. B. Decrease k_5 10 times. C. Increase k_{-5} 10 times. D. Increase k_{-5} 10 times.</p>	<p>A. Unstable points between A and B in Fig. 1c shift to the right. The size of the unstable region increases.</p> <p>B. Unstable points between A and B in Fig. 1c regions shift to the left. The size of the unstable region decreases.</p> <p>C. Unstable points between A and B in Fig. 1c regions shift to the left. The size of the unstable region decreases. Maximum Ras activation increases a little. See Fig. S3d.</p> <p>D. Unstable points between A and B in Fig. 1c regions shift to the right. The size of the unstable region increases. See Fig. S3d.</p> <p>No qualitative changes.</p>
Ras concentration	<p>A. Increased 2 times B. Decreased 2 times</p> <p>Note, changing Ras concentration by 10 times amounts to changing the cell</p>	<p>A. Maximum Ras activation is increased about two times; the unstable region between A and B in Fig. 1c is expanded, especially near region B.</p>

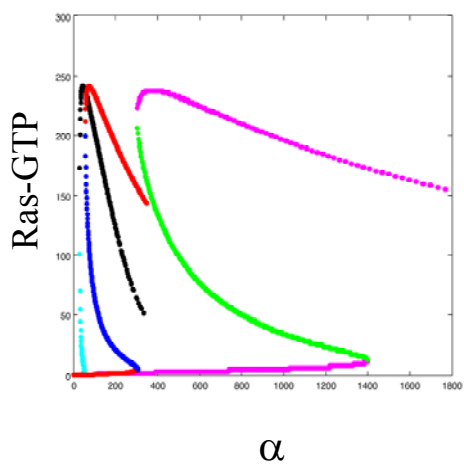
	<p>surface area 10 times which is not realistic. Therefore, we vary the Ras concentration 2 fold.</p>	<p>B. Maximum Ras activation decreased more than two times; the unstable region between A and B in Fig. 1c is shrunk, especially near region B. Details are shown in Fig. S4a.</p> <p>No qualitative changes.</p>
RasGAP concentration	<p>A. Increased 2 times B. Decreased 2 times</p> <p>Note, changing RasGAP concentration by 10 times amounts to changing the cell volume 10 times which is not realistic. Therefore, we vary the RasGAP concentration 2 fold.</p>	<p>A. Unstable points between A and B in Fig. 1c shift to the right. The size of the unstable region increases. Maximum Ras activation decreases.</p> <p>B. Unstable points between A and B in Fig. 1c regions shift to the left. The size of the unstable region decreases and maximum Ras activation increases. Details are shown in Fig. S4b.</p> <p>No qualitative changes.</p>



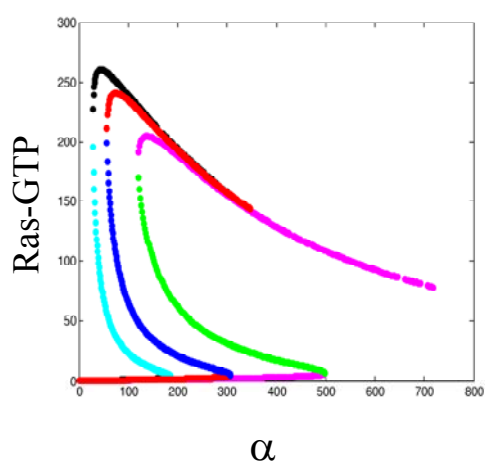
(a)



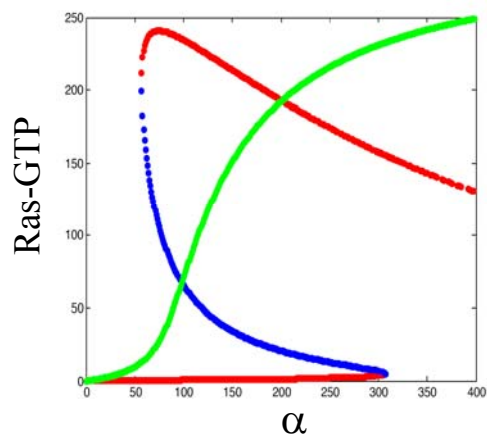
(b)



(c)



(d)



(e)

Fig. S2 Effects of variations of parameters in Fig. 1c: (a) The base case in Fig. 1c in the main text is reproduced here for comparison. (b) k_1 is increased (cyan (unstable) and black (stable) points) and decreased (green (unstable) and magenta (stable) points) 10 folds. (c) k_2 is increased (cyan (unstable) and black (stable) points) and decreased (green (unstable) and magenta (stable) points) 10 folds. (d) k_3^{cat} is increased (cyan (unstable) and black (stable) points) and decreased (green (unstable) and magenta (stable) points) 2 folds. The base case (red and blue) is shown for comparison in (b), (c) and (d). Note that the scale on each panel is different. (e) The unstable fixed points disappear (data shown in green) if the allosteric pocket of SOS_{cat} is mutated in a way that it cannot bind to Ras-GDP or Ras-GTP. The catalytic rate (k_{cat}) through SOS in this case is very small ($\sim 0.0005 \text{ s}^{-1}$), however, in order to keep the data in the same panel as the wild type, we increased the k_{cat} to 0.038 s^{-1} . The wildtype data is shown in red and blue.

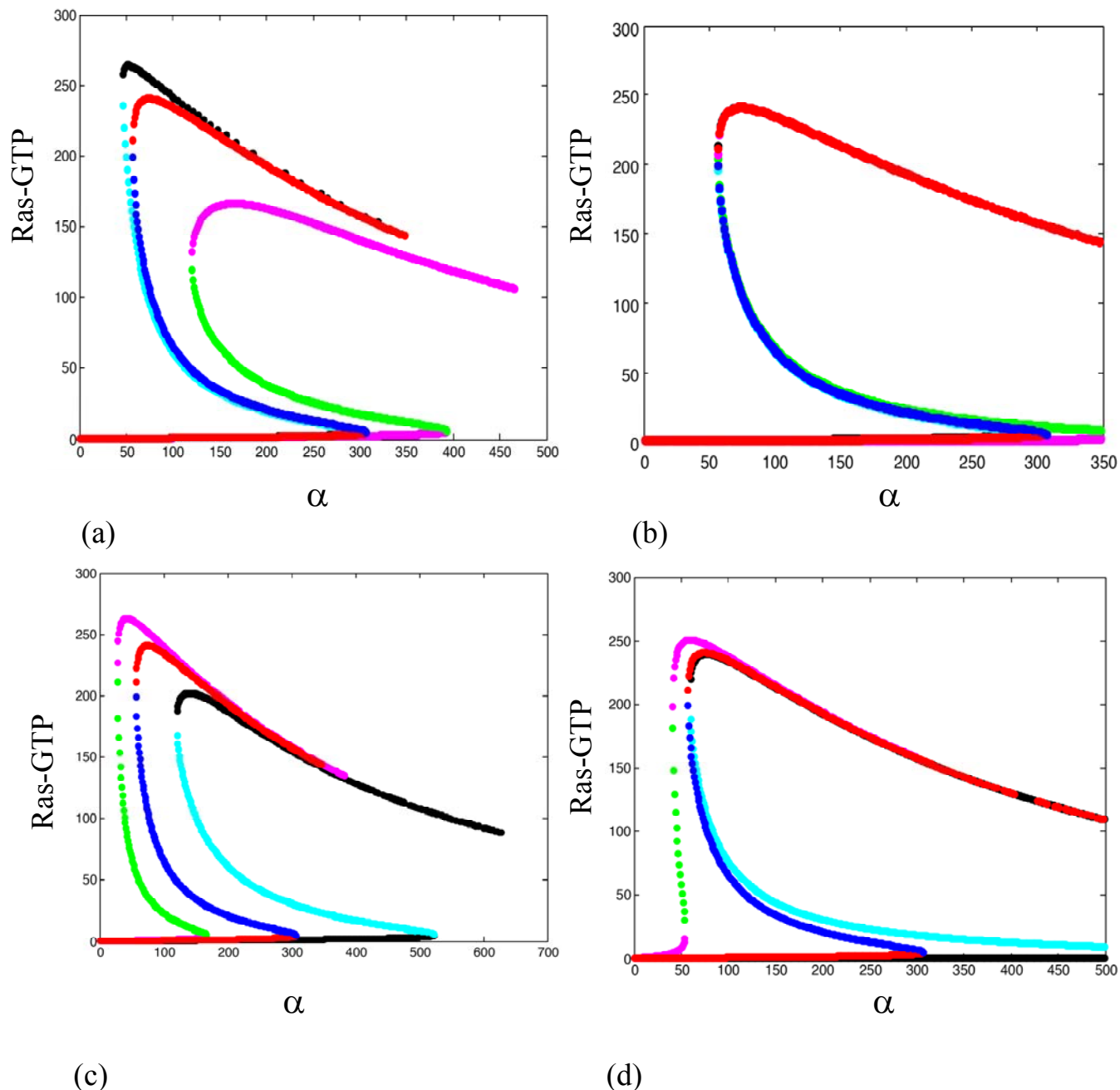


Fig. S3 Effects of variations of parameters in Fig. 1c: (a) k_3 is increased (cyan (unstable) and black (stable) points) and decreased (green (unstable) and magenta (stable) points) by a factor of 10. (b) k_4 is increased (cyan (unstable) and black (stable) points) and decreased (green (unstable) and magenta (stable) points) 10 folds. (c) k_5^{cat} is increased (cyan (unstable) and black (stable) points) and decreased (green (unstable) and magenta (stable) points) by a factor of 2. (d) k_5 is increased (cyan (unstable) and black (stable) points) and decreased (green (unstable) and magenta (stable) points)

10 folds. The base case (red and blue) is shown for comparison in (a), (b), (c) and (d).

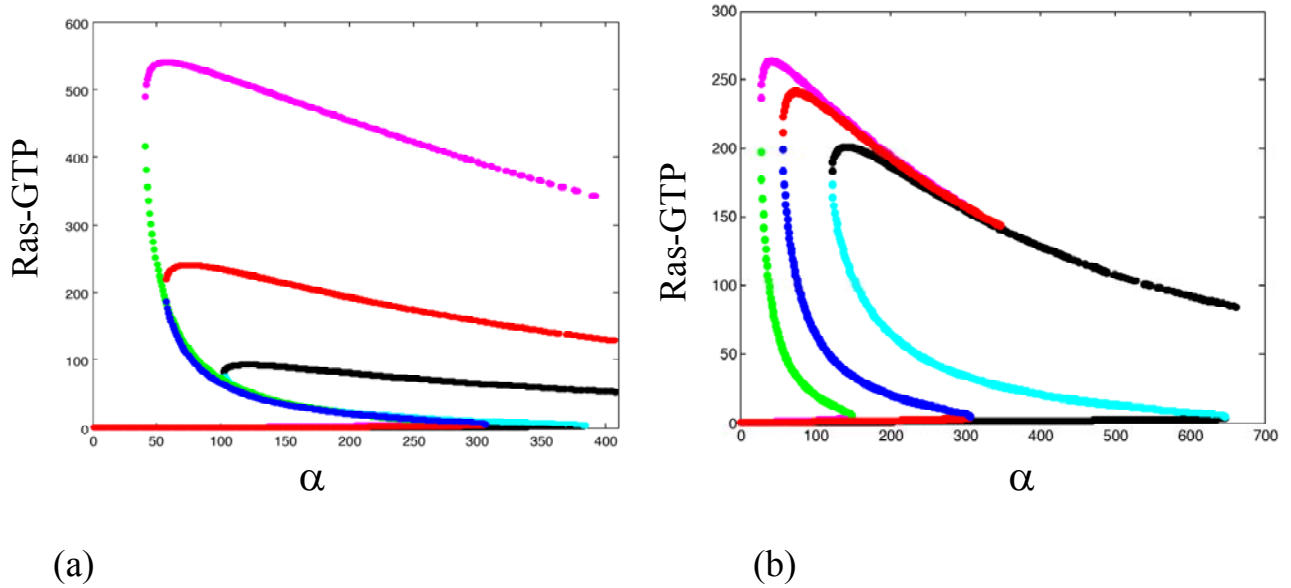


Fig. S4 Effects of variations of concentrations in Fig. 1c: (a) Ras concentration is increased (green (unstable) and magenta (stable) points) and decreased (cyan (unstable) and black (stable) points) by a factor of 2. The base case (Fig. 1c) is displayed in all the plots for comparison. (b) Ras-GAP concentration is decreased (green (unstable) and magenta (stable) points) and increased (cyan (unstable) and black (stable) points) by a factor of 2. The base case (Fig. 1c) is displayed in all the plots for comparison.

Section II. Stochastic Simulation of the Network in Figure 2a:

We perform a stochastic simulation which effectively solves the Master equation (14) corresponding to the stochastic events involved in the chemical reactions in the signaling network shown in Fig. 2a. This simulation technique is also known as the Gillespie method in the literature, and has been widely used for studying stochastic effects in chemical reactions. More technical details of this technique can be found in Refs.(15-17). We choose a simulation box shown in Fig. S1. The volume V and the surface area of the box are taken to be $0.08 (\mu\text{m})^3$ and $2.0 \times 2.0 (\mu\text{m})^2$. The known diffusion time scales of the species ($\sim 1 (\mu\text{m})^2/\text{s}$ (2) in the plasma membrane and $\gg 1 (\mu\text{m})^2/\text{s}$ in the cytosol (18)) involved in the signaling reactions is much faster than their reaction time scales; therefore, we assume that all the species are distributed homogeneously in our simulation box. For all the reactions involving membrane proteins we use a 2D binding rate $(k_{\text{on}})_{2\text{D}}$ calculated from a 3D binding rate $(k_{\text{on}})_{3\text{D}}$. For any other reactions we use the 3D binding rates. Below we show the procedure for calculating $(k_{\text{on}})_{2\text{D}}$ from $(k_{\text{on}})_{3\text{D}}$.

Calculation of $(k_{\text{on}})_{2\text{D}}$ from $(k_{\text{on}})_{3\text{D}}$:

A convenient way of calculating $(k_{\text{on}})_{2\text{D}}$ would be to divide $(k_{\text{on}})_{3\text{D}}$ by a length-scale (d) in which the reactions take place. We take that length scale to be of the order of the radius of gyration of a Ras molecule $\sim 1.7 \text{ nm}$ (1). We will use this for all the reactions taking place in the plasma membrane. In this way, $(k_{\text{on}})_{3\text{D}} = 1 \text{ M}^{-1}\text{s}^{-1} = 0.16 \times 10^{-8} (\mu\text{m})^3/\text{molecules s}^{-1}$ will give us, $(k_{\text{on}})_{2\text{D}} = 0.16 \times 10^{-8} (\mu\text{m})^3/1.7 \text{ nm molecules}^{-1} \text{ s}^{-1} = 0.00941 \times 10^{-4} (\mu\text{m})^2 \text{ molecules}^{-1} \text{ s}^{-1}$.

Simulations for SOS_{cat} transfection: The reactions and rate constants, and the concentrations of the species used are shown in tables S1, S4 and S5. Except for Rasgrp1, SOS and Ras-GAP all other species are taken to be plasma membrane bound. We perform a detailed parameter sensitivity analysis for the parameters which are not measured or measured in *in-vitro* experiments (Tables S7-S8).

Table S4: Reactions and Rate constants for SOS_{cat} transfection simulations

Reaction	k_{on} (μM) ⁻¹ s ⁻¹	k_{off} (s ⁻¹)	$K_D=k_{off}/k_{on}$ (μM)	k_{cat} (s ⁻¹)
6. (catalytic pocket reaction) SOS + Ras - GDP \leftrightarrow SOS - Ras - GDP \rightarrow SOS + Ras - GTP	0.27	4.0	14.5 Ref. (3)	0.0005 Ref. (4)
7. (DAG binding of Rasgrp1) DAG + Rasgrp1 \leftrightarrow DAG - Rasgrp1	5.0	5.0	1.0	
8. (activation by Rasgrp1) DAG - Rasgrp1 + Ras - GDP \leftrightarrow DAG - Rasgrp1 - Ras - GDP \rightarrow DAG - Rasgrp1 + Ras - GTP	0.33	1.0	3.0 (rate known for Rasgrp1) Ref. (19)	0.01 (rate known for Rasgrp1) Ref. (19)
9. (deactivation by Ras) Ras - GTP \rightarrow Ras - GDP				0.0004 Ref. (7)

Table S5: Concentrations used for SOS_{cat} transfection simulations

Species	Concentrations
Ras	75 molecules/ $(\mu\text{m})^2$
SOS _{cat}	Varied from 0 to 1900 molecules/ $(\mu\text{m})^3$ in the SOS _{cat} transfection simulations.
Rasgrp1	Varied from 0 to 1250 molecules/ $(\mu\text{m})^3$ in the SOS _{cat} transfection simulations.
DAG	12 molecules/ $(\mu\text{m})^2$
Ras-GAP	125 molecules/ $(\mu\text{m})^3$

Please note, none of the concentrations are known for lymphocytes. However, some concentrations of these species have been measured or estimated (not measured experimentally) in the literature and vary widely between cell types. This is shown in Table S3. We used these values to estimate the numbers we have used in our simulation and we perform a parameter sensitivity to show the robustness of our results to variations of

these parameters (Table S8). For values of Ras and RasGAP concentrations, the comments made in Sec. I apply.

Table S6: Parameter sensitivity for SOS_{cat} transfections simulations: rate constants measured for related molecules or unknown

The rate constants that are not measured in experiments are varied. In many cases the K_D values of reactions are known, but the binding and the unbinding rates are not known, for those cases, we vary k_{on} and k_{off} at the same time keeping the K_D fixed. We study the sensitivity of the results shown in Fig. 2b upon these variations; we particularly choose the cell distribution for intermediate SOS_{cat} transfection for the wild type cells for this study, because it captures the salient points of the Ras activation dynamics in these experiments. We also study the sensitivity of the hysteresis in Ras activation which is shown in Fig. 6a in the main text. We also study the variations of the rate constants that are measured in vitro, because, their values can change in in-vivo environments, these results are shown in Table S8.

Reaction #	Parameter (s)	Parameter Variation	RasGTP levels	Hysteresis
1.	k_1 and k_{-1} (K_D measured in-vitro)	A. increased 10 times B. decreased 10 times	Active Ras cell population in Fig. 2b for intermediate SOS_{cat} transfections for the wt, decreased a little (for A) or increased a little (for B). Qualitative features of the distributions are not changed.	The range of SOS_{cat} that gives hysteretic behavior in Fig. 6a, moved to the right a little (for A), or, moved to the left a little (for B). Qualitative behavior is unchanged.

2.	k_2 and k_{-2} (K_D measured in-vitro)	A. increased 10 times. B. decreased 10 times.	Active Ras cell population in Fig. 2b for intermediate levels of SOScat transfections in wt cells decreased a little for both A and B. The changes are shown in Fig. S5a. Qualitative features of the distributions are not changed.	The range of SOS_{cat} that gives hysteretic behavior in Fig. 6a, moved to the right and expanded a little (for A), or, moved to the right and expanded a little (for B). Details shown in Fig. S5b. Qualitative features are not changed.
3.	k_3 and k_{-3} (K_D measured in-vitro)	A. increased 10 times B. decreased 10 times	Active Ras cell population in Fig. 2b for intermediate levels of SOScat in wt increased (for A), or, decreased and the Ras activation slowed down, i.e., the bimodality in Ras	The range of SOS_{cat} that gives hysteretic behavior in Fig. 6a moved to the left (for A), or, moved to the right and expanded (for B). Qualitative

			<p>distribution for the base case occurred at a later time point (for B).</p> <p>Qualitative features of the distributions are not changed.</p>	<p>features are not changed.</p>
4.	k_4	<p>A. increased 10 times.</p> <p>B. decreased 10 times</p>	<p>Active Ras cell population in Fig. 2b for intermediate levels of SOS_{cat} transfections in wt cells increased (for A), or, decreased (for B).</p> <p>Qualitative features of the distributions are not changed.</p>	<p>The range of SOS_{cat} that gives hysteretic behavior in Fig. 6a moved to the left and shrunk a little (for A), or, moved to the right and expanded a little (for B).</p> <p>Qualitative features of the distributions are not changed.</p>
4.	k_{-4}	<p>A. increased 10 times.</p> <p>B. decreased</p>	<p>Similar behavior observed as in the previous</p>	<p>The range of SOS_{cat} that gives hysteretic</p>

		10 times.	case for B and A respectively. Qualitative features of the distributions are not changed.	behavior in Fig. 6a moved to the right and expanded (for A), or, moved to the left and shrunk a little (for B). Qualitative features are not changed.
5.	k_5	A. increased 2-10 times. B. decreased 2-10 times. The comments in the last two columns for this parameter are for 2 fold changes. Upon changing the value 10 fold, the region of bistability and hysteresis falls in unrealistic values of species concentrations, but there is no qualitative changes in	Active Ras cell population in Fig. 2b for intermediate levels of SOS _{cat} in wt cells is decreased (for A). The bimodal distribution occurs at a larger SOS _{cat} concentration. The active Ras cell population is increased. The bimodal distribution occurs at a smaller SOS _{cat} concentration at a smaller	The range of SOS _{cat} that gives hysteretic behavior in Fig. 6a moved to the left, and shrunk (for A), or, moved to the right and expanded (for B). Qualitative features are not changed.

		results.	level of Rasgrp1 (for B). Qualitative features of the distributions are not changed.	
5.	k_{-5}	A. increased 2-10 times. B. decreased 2-10 times The comments in the last two columns for this parameter are for 2 fold changes. Upon changing the value 10 fold, the region of bistability and hysteresis falls in unrealistic values of species concentrations, but there is no qualitative change in results.	Same as in the previous case for B. Same as in the previous case for A.	Same as in the previous case for B. Same as in the previous case for A.
5.	k_5^{cat} (k_5^{cat} measured in-vitro for p120 RasGAP)	A. increased 2 times. B. decreased 2 times.	Active Ras cell population in Fig. 2b for intermediate levels of	The range of SOS_{cat} that gives hysteretic behavior in

		<p>The comments in the last two columns for this parameter are for 2 fold changes because we use a measured value. Upon changing the value 10 fold, the region of bistability and hysteresis falls in unrealistic values of species concentrations, but there is no qualitative change in results.</p>	<p>SOScat in wt is decreased (for A). The bimodal distribution occurs at a larger SOScat concentration.</p> <p>For B, the active Ras cell population is increased. The bimodal distribution occurs at a smaller SOScat concentration.</p> <p>Qualitative features of the distributions are not changed.</p>	<p>Fig. 6a moved to the right, and expanded (for A), or, moved to the left and shrunk (for B).</p> <p>Qualitative features do not change.</p>
6.	k_6 and k_{-6} (K_D measured <i>in-vitro</i>)	<p>A. increased 10 times.</p> <p>B. decreased 10 times.</p>	<p>Active Ras cell population in Fig. 2b for intermediate SOScat transfections for the wt, decreased a little (for A) or increased a little (for B).</p> <p>Qualitative features of the</p>	<p>The range of SOS_{cat} that gives hysteretic behavior in Fig. 6a, moved to the right a little (for A), or, moved to the left a little (for B).</p>

			distributions are not changed.	Qualitative behavior is unchanged.
7.	k_7	<p>A. increased 2-10 times.</p> <p>B. decreased 2-10 times.</p> <p>The comments in the last two columns for this parameter are for 2 fold changes. Upon changing the value 10 fold, the region of bistability and hysteresis falls in unrealistic values of species concentrations, but there is no qualitative change in results.</p>	<p>Active Ras cell population</p> <p>In Fig. 2b for intermediate levels of SOS_{cat} in wt cells is increased and the Ras activation becomes much faster, therefore, the bimodal distribution in cell population occurs at an earlier time(for A) (Fig. S6a). For B the population level at active Ras is decreased, the Ras activation is slowed down, i.e., the bimodality in Ras distribution for the base case occurs at a later time point (Fig. S6a).</p>	<p>The range of SOS_{cat} that gives hysteretic behavior in Fig. 6a, moved to the left, and shrinks a little (for A), or, moved to the right and is expanded (for B). Details in Fig. S6b.</p> <p>Qualitative features of the hysteresis are not changed.</p>

			Qualitative features of the distributions are not changed.	
7.	k_7	<p>A. increased 2-10 times B. decreased 2-10 times</p> <p>The comments in the last two columns for this parameter are for 2 fold changes. Upon changing the value 10 fold, the region of bistability and hysteresis falls in unrealistic values of species concentrations, but there is no qualitative change in results.</p>	<p>Same as in the previous case for B.</p> <p>Same as in the previous case for A.</p> <p>Qualitative features of the distributions are not changed.</p>	<p>Same as in the previous case for B.</p> <p>Same as in the previous case for A.</p> <p>Qualitative features of the hysteresis are not changed.</p>
8.	k_8	<p>A. increased 2-10 times B. decreased 2-10 times</p> <p>The comments in the last two columns for this parameter</p>	<p>Active Ras cell population in Fig. 2b for intermediate levels of SOS_{cat} in wt cells is increased, the Ras activation</p>	<p>The range of SOS_{cat} that gives hysteretic behavior in Fig. 6a moved to the left, and shrinks a</p>

		<p>are for 2 fold changes. Upon changing the value 10 fold, the region of bistability and hysteresis falls in unrealistic values of species concentrations, but there is no qualitative change in results.</p>	<p>becomes much faster, therefore, the bimodal distribution in cell population occurs at an earlier time (for A). The active Ras cell population is decreased, the Ras activation is slowed down, i.e., the bimodality in Ras distribution for the base case occurs at a later time point (for B).</p> <p>Qualitative features of the distributions are not changed.</p>	<p>little (for A), or, moved to the right and is expanded (for B).</p> <p>Qualitative features are not changed.</p>
8.	k ₈	<p>A. increased 2-10 times.</p> <p>B. decreased 2-10 times.</p> <p>The comments in the last two columns for</p>	<p>Same as the previous case for change B.</p> <p>Same as the previous case for change A.</p> <p>Qualitative</p>	<p>Same as the previous case for change B.</p> <p>Same as the previous case for change A.</p>

		<p>this parameter are for 2 fold changes. Upon changing the value 10 fold, the region of bistability and hysteresis falls in unrealistic values of species concentrations, but there is no qualitative change in results.</p>	<p>features of the distributions are not changed.</p>	<p>Qualitative features do not change.</p>
8.	k_8^{cat} (measured <i>in-vitro</i> for Rasgrf1)	<p>A. increased 2 times. B. decreased 2 times.</p> <p>The comments in the last two columns for this parameter are for 2 fold changes because we use a measured value. Upon changing the value 10 fold, the region of bistability and hysteresis falls in unrealistic values of</p>	<p>Active Ras cell population in Fig. 2b for intermediate SOS_{cat} levels in wt cells is increased for A. The Ras activation becomes much faster, therefore, the bimodal distribution in cell population occurs at an earlier times and at lower levels of Rasgrp1. For B, the population at high Ras</p>	<p>The range of SOS_{cat} that gives hysteretic behavior in Fig. 6a moved to the left, and shrunk (for A), or, moved to the right and expanded (for B).</p> <p>Qualitative features are not changed.</p>

		<p>species concentrations, but there is no qualitative change in results.</p>	<p>activation is decreased, the Ras activation is slowed down, i.e., the bimodality in Ras distribution case occurs at later time points at higher Rasgrp1 concentrations.</p> <p>Qualitative features of the distributions are not changed.</p>	
--	--	---	--	--

Table S7: Parameter sensitivity for concentrations used for SOS_{cat} transfection simulations

Species	Variation	Effect on cell Population	Effect on cell hysteresis
Ras	<p>A. 2 times increase.</p> <p>B. 2 times decrease.</p> <p>Note, changing Ras concentration by 10 times amounts to changing the cell surface area 10 times which is not realistic. Therefore, we vary the Ras concentration 2 fold.</p>	<p>The bimodal distribution in cell population for intermediate levels of SOS_{cat} in wt cells (Fig. 2b) is observed at a lower SOS_{cat} level and the maximal Ras activation goes up (for A). The bimodal distribution is seen at a higher SOS_{cat} level and the maximal Ras activation goes down (for B). Details shown in Fig. S7a.</p> <p>Qualitative features of the distributions are not changed.</p>	<p>The range of SOS_{cat} that gives hysteretic behavior in Fig. 6a, moved to the left and maximal Ras activation goes up, or, moved to the right and expanded (for B). Maximal Ras activation goes down for B.</p> <p>Qualitative features of the distributions are not changed.</p> <p>Details shown in Fig. S7b.</p> <p>Qualitative features are not altered.</p>
DAG	<p>A. 2 times increase.</p> <p>B. 2 times decrease.</p> <p>Note, changing DAG concentration by 10</p>	<p>Active Ras cell population for intermediate SOS_{cat} concentration (Fig. 2b) in wt</p>	<p>The range of SOS_{cat} that gives hysteretic behavior in Fig. 6a moved to the left and shrunk</p>

	<p>times amounts to changing the cell surface area 10 times which is not realistic. Therefore, we vary the DAG concentration 2 fold.</p>	<p>cells is observed to increase, the bimodal distribution occurs at an earlier time point for A.</p> <p>For B, the cell population at active Ras decreases and the bimodal distribution occurs at a later time point.</p> <p>Qualitative features of the distributions are not changed.</p>	<p>(for A), or, moved to the right and expanded (for B).</p> <p>Qualitative features do not change.</p>
Ras-GAP	<p>A. 2 times increase. B. 2 times decrease.</p> <p>Note, changing RasGAP concentration by 10 times amounts to changing the cell volume 10 times which is not realistic. Therefore, we vary the RasGAP concentration 2 fold.</p>	<p>1. Active Ras cell population in Fig. 2b for wt is observed at a 1. higher SOS_{cat} level and amount of Ras activation goes down. 2. lower SOS_{cat} level and low amount of Rasgrp1 level. Maximum of Ras activation goes down. Details in Fig. S8a.</p>	<p>The range of SOS_{cat} that gives hysteretic behavior in Fig. 6a moved to the left and shrunk (for A), or, moved to the right and expanded (for B). The maximal Ras activation increased and decreased for A and B respectively.</p>

		Qualitative features of the distributions are not changed.	Details in Fig. S8b. Qualitative features do not change.
--	--	--	---

Table S8: Parameter sensitivity for SOS_{cat} transfections simulations: rate constants measured for the pertinent molecules

Here we vary the parameters that have been measured outside the cell because they may vary in the cellular environment.

Reaction	Parameter	Parameter Variation	Effect on cell population	Effect on cell hysteresis
1.	k_1	A. 10 times increase. B. 10 times decrease.	The rate of Ras activation decreases for (A) and increases for (B). The value of the intermediate level of SOS _{cat} that gives rise to bimodal behavior is increased and decreased respectively for (A) and (B). Qualitative features are not changed.	The range of SOS _{cat} that gives hysteretic behavior in Fig. 6a, moved to the right, and expands (for A), or, moved to the left and is shrunk (for B). Qualitative features of the hysteresis are not changed.
1.	k_{-1}	A. 10 times increase. B. 10 times decrease.	Same as the previous case for change B. Same as the previous case for change A. Qualitative	Same as the previous case for change B. Same as the previous case for change A.

			features do not change.	Qualitative features do not change.
2.	k_2	<p>A. 2 times increase.</p> <p>B. 2 times decrease.</p> <p>We vary this parameter by factors of 2 only because we use its value measured <i>in-vitro</i>. By changing it 10 times, the region of bistability will fall in unrealistic values of species concentrations, but the bistability remains.</p>	<p>The rate of Ras activation increases for (A) and decreases for (B). The value of the intermediate level of SOS_{cat} that gives rise to bimodal behavior is decreased a little for (A). Qualitative features are not changed.</p> <p>Details in Fig. S9a.</p>	<p>The range of SOS_{cat} that gives hysteretic behavior in Fig. 6a, moved to the left, and shrunk (for A), or, moved to the right and expanded (for B). Qualitative features of the hysteresis are not changed.</p> <p>Details in Fig. S9b.</p>
2.	k_{-2}	<p>A. 2 times increase.</p> <p>B. 2 times decrease.</p> <p>We vary this parameter by</p>	<p>Same as the previous case for change B.</p> <p>Same as the previous case for change A.</p>	<p>Same as the previous case for change B.</p> <p>Same as the previous case for</p>

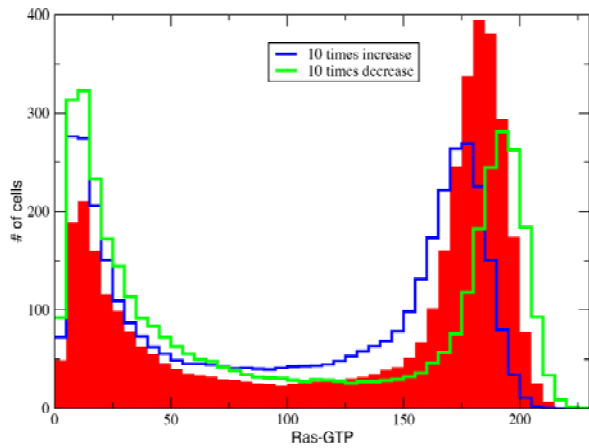
		factors of 2 only because we use its value measured <i>in-vitro</i> . By changing it 10 times, the region of bistability will fall in unrealistic values of species concentrations, but the bistability remains.	Qualitative features do not change.	change A. Qualitative features do not change.
3.	k_3	A. 10 times increase. B. 10 times decrease.	The rate of Ras activation increases for (A) and decreases for (B). The value of the intermediate level of SOS _{cat} that gives rise to bimodal behavior is decreased or increased for (A) or (B) respectively. Qualitative features are not changed.	The range of SOS _{cat} that gives hysteretic behavior in Fig. 6a, moved to the left, and shrunk (for A), or, moved to the right and expanded (for B). Qualitative features of the hysteresis are not changed.

			Details in Fig. S10a.	Details in Fig. S10b.
3.	k_{-3}	A. 10 times increase. B. 10 times decrease.	Same as the previous case for change B. Same as the previous case for change A. Qualitative features do not change.	Same as the previous case for change B. Same as the previous case for change A. Qualitative features do not change.
3.	k_3^{cat}	A. 2 times increase. B. 2 times decrease. We vary this parameter by factors of 2 only because we use its value measured <i>in-vitro</i> . By changing it 10 times, the region of bistability will fall in unrealistic values of species concentrations,	The rate of Ras activation increases for (A) and decreases for (B). The value of the intermediate level of SOS _{cat} that gives rise to bimodal behavior is decreased or increased for (A) or (B) respectively. Qualitative features are not changed. Details in Fig.	The range of SOS _{cat} that gives hysteretic behavior in Fig. 6a, moved to the left, and shrinks (for A), or, moved to the right and is expanded (for B). The maximal Ras activation increases and decreases for (A) and (B)

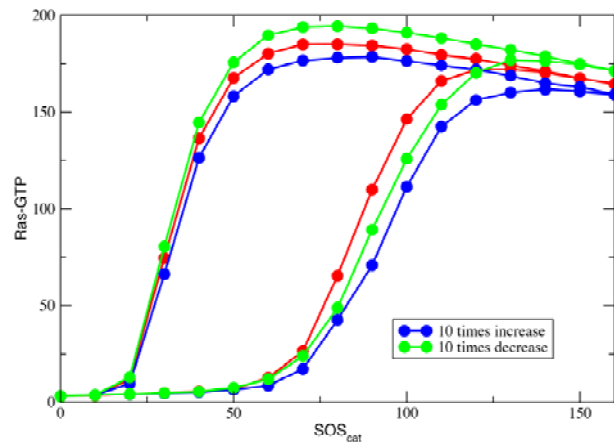
		but the bistability remains.	S11a.	respectively. Qualitative features of the hysteresis are not changed. Details in Fig. S11b.
4.	k_4^{cat}	<p>A. 2 times increase.</p> <p>B. 2 times decrease.</p> <p>We vary this parameter by factors of 2 only because we use its value measured <i>in-vitro</i>. By changing it 10 times, the region of bistability will fall in unrealistic values of species concentrations, but the bistability remains.</p>	<p>The rate of Ras activation increases for (A) and decreases for (B). The value of the intermediate level of SOS_{cat} that gives rise to bimodal behavior is decreased a little for (A). Qualitative features are not changed.</p> <p>Details in Fig. S12a.</p>	<p>The range of SOS_{cat} that gives hysteretic behavior in Fig. 6a, moved to the left, and shrunk a little (for A), or, moved to the right and expanded a little (for B). Qualitative features of the hysteresis are not changed.</p> <p>Details in Fig. S12b.</p>
6.	k_6	<p>A. 10 times increase.</p> <p>B. 10 times</p>	<p>The rate of Ras activation increases for</p>	<p>The range of SOS_{cat} that gives</p>

		decrease.	(A) and decreases for (B). The value of the intermediate level of SOScat that gives rise to bimodal behavior is decreased and increased respectively for (A) and (B). Qualitative features are not changed.	hysteretic behavior in Fig. 6a, moved to the left, and shrinks (for A), or, moved to the right and is expanded (for B). Qualitative features of the hysteresis are not changed.
6.	k_6	A. 10 times increase. B. 10 times decrease.	Same as the previous case for change B. Same as the previous case for change A. Qualitative features do not change.	Same as the previous case for change B. Same as the previous case for change A. Qualitative features do not change.
6.	k_6^{cat}	A. 2 times increase. B. 2 times decrease. We vary this parameter by factors of 2	Very little change in the distributions for both (A) and (B). Qualitative features do	Very little change for both (A) and (B). Qualitative features do not change.

		only because we use its value measured <i>in-vitro</i> . By changing it 10 times, the region of bistability will fall in unrealistic values of species concentrations, but the bistability remains.	not change.	
--	--	---	-------------	--

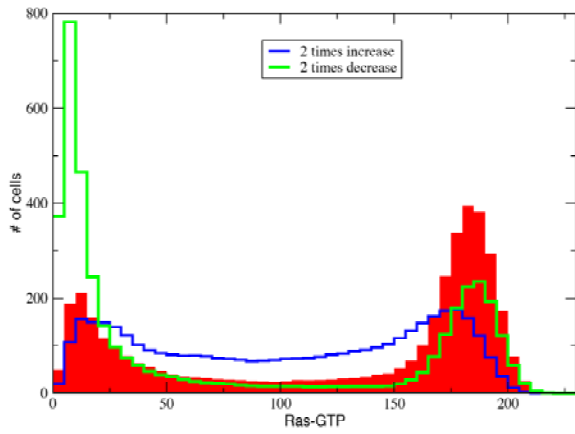


(a)

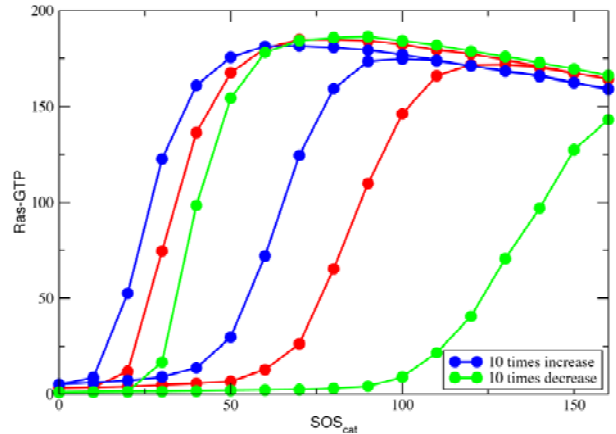


(b)

Fig. S5. Effect of change in the binding (k_2) and unbinding (k_{-2}) rates of RasGTP to the allosteric site of SOS_{cat} : (a) Shows the effect of increasing (blue) and decreasing (green) k_2 and k_{-2} at the same time keeping their ratio fixed, on cell population keeping other parameters fixed as the base case (shown in red). (b) The effects of the same changes as in (a) on the hysteresis pattern of Ras activation. The base case is shown in red. All the data are taken at $t=10$ minutes.

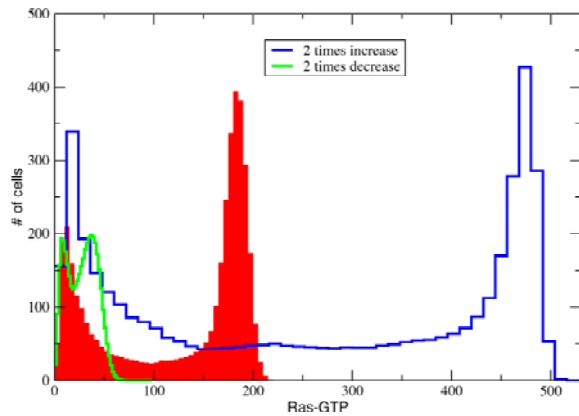


(a)

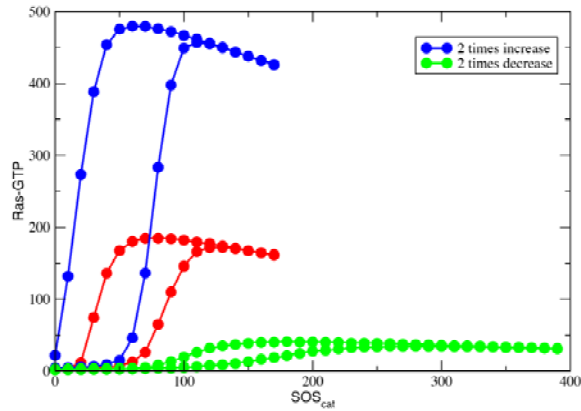


(b)

Fig. S6 Effect of change in the binding rate (k_7) of Rasgrp1 to DAG: (a) k_7 is increased (blue) and decreased (green) two times from the base case shown in red. The same bimodal behavior is observed at earlier times (at 10 mins) and later times (at 20 mins) when k_7 is increased and decreased respectively. The base case is observed at 15 mins. (b) k_7 is increased (blue) and decreased (green) ten times from the base case shown in red. All the data are taken at $t=10$ minutes.



(a)



(b)

Fig. S7 Effect of variation of Ras concentration: Concentration of Ras is increased (blue) and decreased (green) by 2 folds from the base case (red). (a) The same bimodal distribution as in the base case is observed at a lower (0.83 times) and a higher (2 times) SOS_{cat} concentration as the Ras concentration was increased and decreased respectively. (b) Shows the changes in the hysteresis in Ras activation. All the data are taken at $t=10$

minutes. Decreasing Ras concentration seems to lower the effect of hysteresis and bimodality, we have used a lower than estimated values of Ras concentration as our base case, which is a conservative estimate of the parameter.

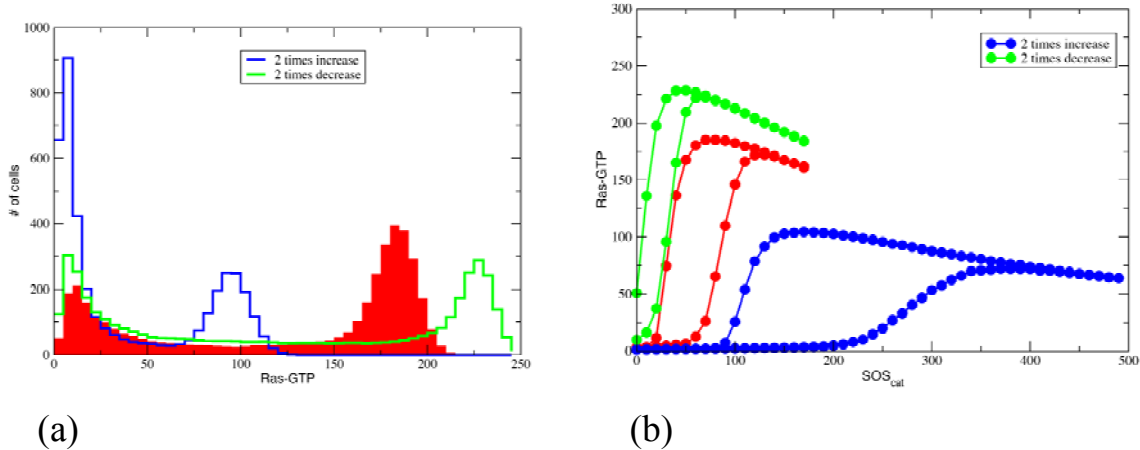
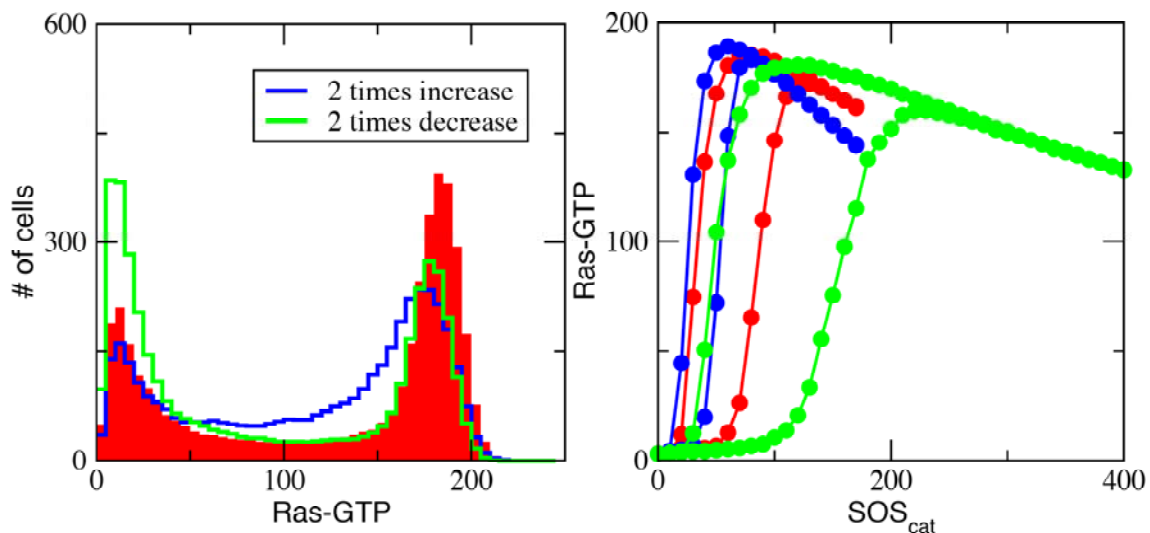


Fig. S8 Effect of variation of Ras-GAP concentration: Concentration of Ras-GAP is increased (blue) and decreased (green) by 2 folds from the base case (red). (a) The same bimodal distribution as in the base case is observed at a higher (3.28 times) SOS_{cat} concentration as the RasGAP concentration is increased. The bimodal distribution as in the base case occurs at a lower (0.65 times) SOS_{cat} concentration and a lower Rasgrp1 (0.25 times) as the RasGAP concentration is decreased. (b) Data show the change in the hysteresis in Ras activation as RasGAP concentration is varied. All the cases are taken at $t=10$ mins. Increasing RasGAP concentration seems to lower the effect of hysteresis and bimodality, we have used a higher than estimated values of RasGAP concentration as our base case, which is a conservative estimate of the parameter.



(a)

(b)

Fig. S9 Effect of variation of rate (k_2) of Ras-GTP binding to the allosteric site of SOS_{cat} : The binding rate (k_2) of Ras-GTP to the allosteric site of SOS_{cat} is increased (blue) and decreased (green) by 2 folds from the base case (red). The same bimodal distribution as in the base case is observed at a lower (0.59 times) SOS_{cat} concentration and a higher (1.73 times) SOS_{cat} concentration as k_2 was increased and decreased respectively. (b) Show the change in the hysteresis of Ras activation. All the cases are taken at $t=10$ mins.

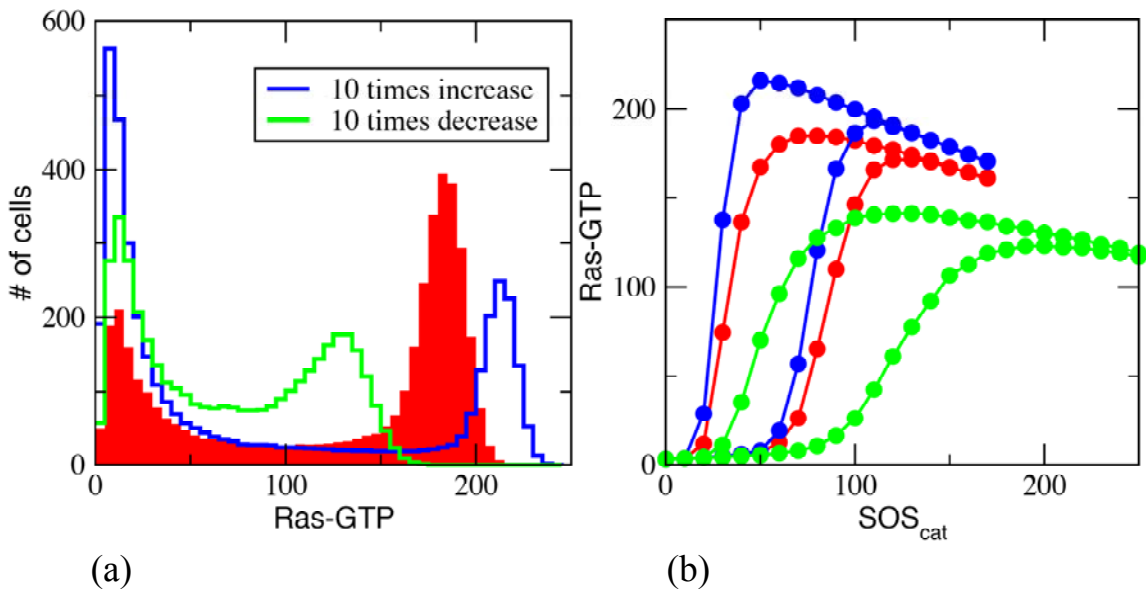


Fig. S10 Effect of variation of the binding rate (k_3) of Ras-GDP to the catalytic pocket of SOS_{cat} when the allosteric site of SOS_{cat} is occupied by Ras-GTP: The catalytic rate (k_3) is increased (blue) and decreased (green) by 10 folds from the base case (red). The bimodal distribution as in the base case is observed at a slightly lower (0.85 times) SOS_{cat} concentration and a higher (1.31 times) SOS_{cat} concentration as k_3 was increased and decreased respectively. (b) Show the change in the hysteresis of Ras activation. All the cases are taken at $t=10$ mins.

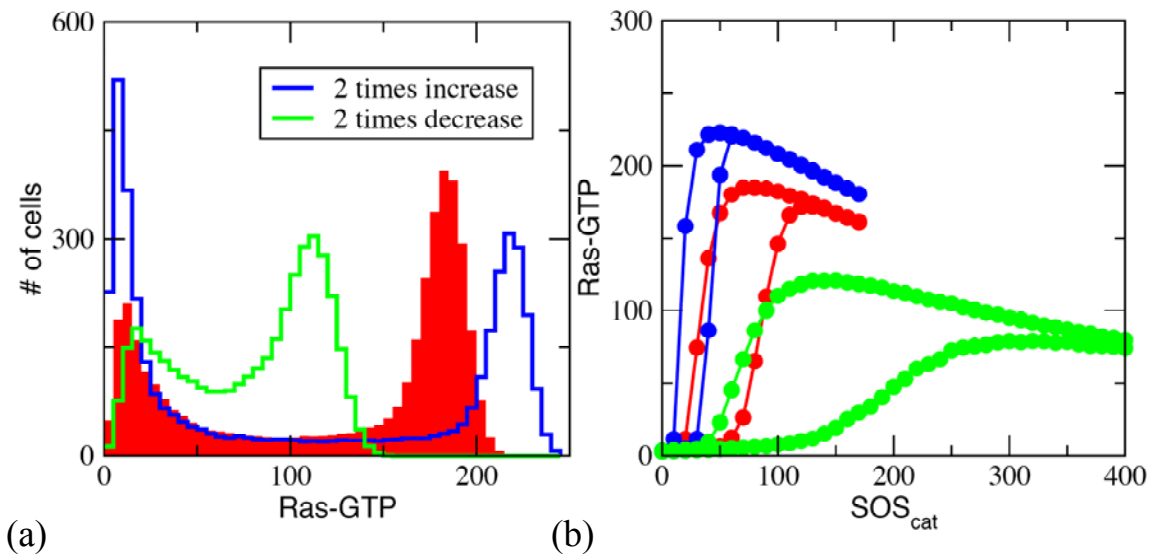


Fig. S11 Effect of variation of catalytic rate (k_3^{cat}) of SOS_{cat} when the allosteric site of SOS_{cat} is occupied by Ras-GTP: The catalytic rate (k_3^{cat}) is increased (blue) and decreased (green) by 2 folds from the base case (red). The bimodal distribution as in the base case is observed at a lower (0.47 times) SOS_{cat} concentration and a higher (2.23) SOS_{cat} concentration as k_3^{cat} was increased and decreased respectively. (b) Show the change in the hysteresis of Ras activation. All the cases are taken at $t=10$ mins.

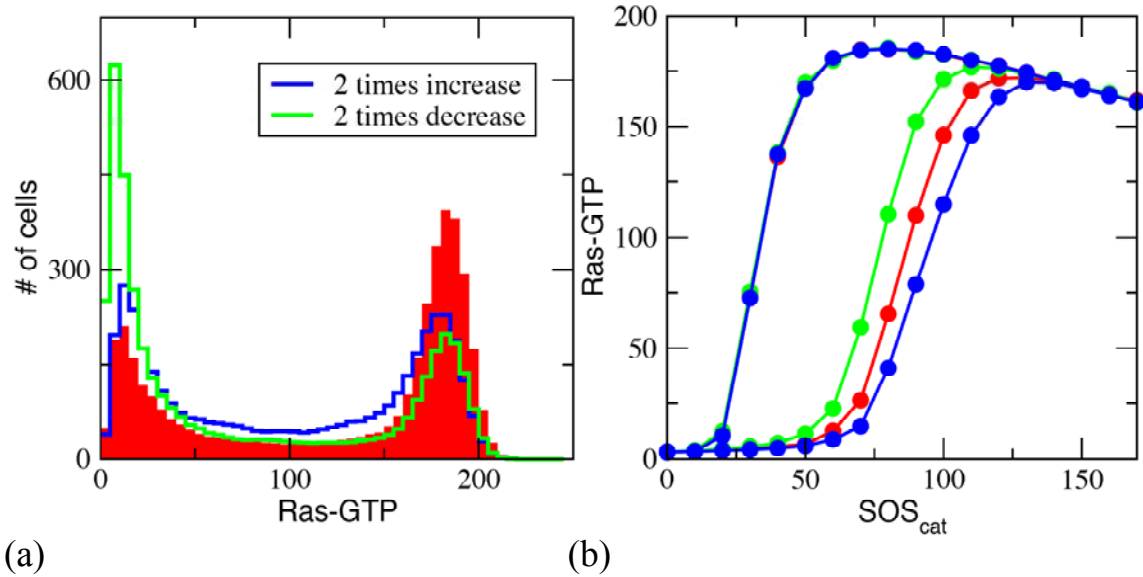


Fig. S12 Effect of variation of catalytic rate (k_4^{cat}) of SOS_{cat} when the allosteric site of SOS_{cat} is occupied by Ras-GDP: The catalytic rate (k_4^{cat}) is increased (blue) and decreased (green) by 2 folds from the base case (red). The bimodal distribution as in the base case is observed at a slightly lower (0.85 times) SOS_{cat} concentration and the same SOS_{cat} concentration as k_4^{cat} was increased and decreased respectively. (b) Show the change in the hysteresis of Ras activation. All the cases are taken at $t=10$ mins.

Section III. Simulations of Receptor Stimulation

We simulate the response to receptor stimulation for the reactions shown in Fig. 4a. Most of the reactions and the rate constants involving SOS_{cat} and RasGRP1 are already shown in Tables S1 and S4. The rest of the reactions and rate constants are shown in Table S9. The species concentrations are shown in Table S4 and Table S10. We do a detailed parameter sensitivity analysis for the rate constants (Table S12), and concentrations (Table S13). We do not analyze the parameter sensitivity for the rate constants that involves reactions with the allosteric and catalytic sites of SOS_{cat} , because we have already studied their sensitivity in Tables S6 and S8. We also do not show the parameter sensitivity of the concentration variables which have been already reported in Table S7. In the case of receptor stimulation, we label some of the binding unbinding, and phosphorylation reactions as follows: For the n th reaction reported in the table, $A + B \xrightleftharpoons[k_{-n}]{k_n} AB \xrightarrow{k_n^f} A^*B$, A^* denotes the phosphorylated A molecule. When the values of the rates are measured in literature we cite the references, otherwise the numbers are estimated.

Table S9: Reactions and Rate constants for receptor stimulation simulations

Reaction	k_{on} (μM) ⁻¹ s ⁻¹	k_{off} (s ⁻¹)	$K_D = k_{\text{off}}/k_{\text{on}}$ (μM)	k_{cat} (s ⁻¹)
10. TCR + pMHC \leftrightarrow TCR – pMHC	0.0022 (20) value quoted is for 2B4 TCR interacting with an MCC (88- 103) peptide MHC.	0.01 (20, 21)	0.45	N/A

11.	TCR - pMHC + Lck \leftrightarrow TCR - pMHC - Lck \rightarrow TCR* - pMHC - Lck	0.297	10	33.6	5.0 (22)
12.	TCR* species + ZAP70 \leftrightarrow TCR* species - ZAP70	135.0	0.11 (22)	0.0008	N/A
13.	TCR - Lck - species - ZAP70 \rightarrow TCR - Lck - species - ZAP70*	N/A	N/A	N/A	5.0 (22)
14.	TCR - ζ^* \rightarrow TCR - ζ	N/A	N/A	N/A	1.0
15.	ZAP70* - species \rightarrow ZAP70 - species	N/A	N/A	N/A	5.0 (22)
16.	LAT + TCR - species - ZAP70* \leftrightarrow TCR - species - LAT - ZAP70*	0.10	0.1	0.94	N/A
17.	TCR - LAT - ZAP70* \leftrightarrow TCR - LAT* - ZAP70*				5.0
18.	TCR - LAT* - ZAP70* \leftrightarrow TCR - LAT - ZAP70*				1.0
19.	TCR - species - LAT* + PLC γ \leftrightarrow TCR - species - LAT* - PLC γ	161.2	1.0	0.0062 value for the site of LAT that binds with highest affinity (23)	N/A
20.	TCR - species - PLC γ \rightarrow TCR - species - PLC γ^*	N/A	N/A	N/A	0.01
21.	TCR - species - PLC γ^* \rightarrow TCR - species - PLC γ	N/A	N/A	N/A	1.0
22.	TCR - species - PLC γ^* + PIP ₂ \leftrightarrow TCR - species - PLC γ^* - PIP ₂ \rightarrow TCR - species - PLC γ^* + DAG + IP ₃	0.10	0.2	1.9	0.0009
23.	IP ₃ \rightarrow IP ₃ + Ca ²⁺	N/A	N/A	N/A	0.1
24.	Ca ²⁺ + CAPRI \rightarrow CAPRI* + Ca ²⁺	1.2x10 ⁻⁷	N/A	N/A	N/A
25.	TCR - species - LAT* + Grb2 \leftrightarrow TCR - species - LAT* - Grb2	1.0	0.008	0.0073 value close to the affinity of site of	N/A

			LAT that binds with highest affinity (23)	
26. SOS+ TCR-species Grb2 ↔ TCR-species SOS- Grb2	1.4	0.6	0.42 (24)	N/A

Table S10: Concentrations used for receptor stimulation simulations

Species	Concentration
TCR	275 molecules/ $(\mu\text{m})^2$ (22) *
pMHC	17-102 molecules/ $(\mu\text{m})^2$
Lck	275 molecules/ $(\mu\text{m})^2$ (22) *
ZAP70	62500 molecules/ $(\mu\text{m})^3$ (22) *
LAT	75 molecules/ $(\mu\text{m})^2$
PLC γ	12500 molecules/ $(\mu\text{m})^3$
Grb2	5000 molecules/ $(\mu\text{m})^3$
PIP2	1250 molecules/ $(\mu\text{m})^2$
SOS	1000 molecules/ $(\mu\text{m})^3$
Rasgrp1	1500 molecules/ $(\mu\text{m})^3$
RasGAP	250 molecules/ $(\mu\text{m})^3$ **
Ras	75 molecules/ $(\mu\text{m})^2$

* These parameters are of the same order as quoted in the literature (see Table S11); for example, for Lck, the known value is 304. The fact that they are not exactly the same is not of concern since we carry out a parameter sensitivity study varying these numbers by factors of 5, which does not lead to any qualitative changes.

** The concentration of RasGAP is higher than the value used in Sec. II, because, upon receptor stimulation RasGAP is recruited to the membrane. Higher values of RasGAP increases the region of hysteresis (see Fig. S8).

Note many of the concentrations used are not known for lymphocytes. However, some concentrations of these species have been measured or

estimated (not measured experimentally) in the literature and vary widely between cell types. This is shown in Table S2 and S11.

Table S11: Measured or estimated values of concentrations in literature for other cells.

Concentrations measured or estimated in literature						
Species	Ref. (9) (HeLa)	Ref. (10) (PC12)	Ref. (11) (HeLa)	Ref. (12) (estimated)	Ref. (13) (hepatocytes in rats)	Ref. (22)
TCR						304 mols/ $(\mu\text{m})^2$
Lck						304 mols/ $(\mu\text{m})^2$
ZAP70						72000 mols/ $(\mu\text{m})^3$
Grb2		600 mols/ $(\mu\text{m})^3$	51 mols/ $(\mu\text{m})^3$	600 mols/ $(\mu\text{m})^3$	51 mols/ $(\mu\text{m})^3$	

The results shown in tables S13 and S14 can be summarized as noted in the main text. Changing the values of the parameters changes the time point at which the bimodality emerges in simulation of wild type systems, and changes the level of receptor stimulation that can compensate for RasGRP1 deficiency.

Table S12: Parameter Sensitivity for the Rate constants for receptor stimulation simulations

Reaction #	Parameter (s)	Parameter Variations	Effect on cell population Distributions	
			Low signal	High Signal
10.	k_{10}	A. increased 10 times. B. decreased 10 times.	A. Very little change. B. Very little change. Qualitative Features unchanged. Fig. S13a for details.	A. Very little change. B. Very little change. Qualitative Features unchanged. Fig. S13b for details.
10.	k_{-10}	A. increased 10 times. B. decreased 10 times.	Very little change for both (A) or (B). Qualitative Features unchanged.	Very little change for both (A) or (B).
11.	k_{11}	A. increased 10 times. B. decreased 10 times.	Hardly any change for (A) or (B). Qualitative features are not altered.	Hardly any change for (A) or (B). Qualitative features are not altered.
11.	k_{-11}	A. increased 10 times. B. decreased 10 times.	Very little change for (A) or (B). Qualitative features are	Very little change for (A) or (B). Qualitative features are

			not altered.	not altered.
11.	k_{11}^{cat}	A. increased 10 times. B. decreased 10 times.	Very little change for (A) or (B). Qualitative features are not altered.	Very little change for (A) or (B). Qualitative features are not altered.
12.	k_{12}	A. increased 10 times. B. decreased 10 times.	Hardly any change for (A) or (B). Qualitative features unchanged.	Hardly any change for (A) or (B). Qualitative features unchanged.
12.	k_{-12}	A. increased 10 times. B. decreased 10 times.	Hardly any change for (A) or (B). Qualitative features unchanged.	Hardly any change for (A) or (B). Qualitative features unchanged.
13.	k_{13}^f	A. increased 10 times. B. decreased 10 times.	Hardly any change for (A) or (B). Qualitative features unchanged.	Hardly any change for (A) or (B). Qualitative features unchanged.
14.	k_{14}^f	A. increased 10 times. B. decreased 10 times.	Very little change for (A) or (B). Qualitative features not changed.	Very little change for (A) or (B). Qualitative features not changed.
15.	k_{15}^f	A. increased 10 times.	Very little change for (A) or (B).	Very little change for (A) or (B).

		B. decreased 10 times.	Qualitative features not changed.	Qualitative features not changed.
16.	k_{16}	A. increased 10 times. B. decreased 10 times.	Very little change for (A) or (B). Qualitative features not changed.	Very little change for (A) or (B). Qualitative features not changed.
16.	k_{16}	A. increased 10 times. B. decreased 10 times.	Very little change for (A) or (B). Qualitative features not changed. Details in Fig. S14a.	Very little change for (A) or (B). Qualitative features not changed. Details in Fig. S14b.
17.	k_{17}^f	A. increased 10 times. B. decreased 10 times.	Very little change for (A) or (B). Qualitative features not changed.	Very little change for (A) or (B). Qualitative features not changed.
18	k_{18}^f	A. increased 10 times. B. decreased 10 times.	Very little change for (A) or (B). Qualitative features not changed.	Very little change for (A) or (B). Qualitative features not changed.
19.	k_{19}	A. increased 10 times. B. decreased 10 times.	Very little change for (A) or (B). Qualitative features are	Very little change for (A) or (B). Qualitative features are

			not changed.	not changed.
19.	k_{19}	A. increased 10 times. B. decreased 10 times.	Ras activation becomes slower for (A) and faster for (B). Details in Fig. S15a. Qualitative features are not changed.	Ras activation becomes slower for (A) and faster for (B). Details in Fig. S15b. Qualitative features are not changed.
20.	k_{20}^f	A. increased 10 times. B. decreased 10 times.	Ras activation becomes faster for (A) and slower for (B). Qualitative features are not changed.	Ras activation becomes faster for (A) and slower for (B). Qualitative features are not changed.
21.	k_{21}^f	A. increased 10 times. B. decreased 10 times.	Ras activation becomes slower for (A) and faster for (B). Qualitative features are not changed.	Ras activation becomes slower for (A) and faster for (B). Qualitative features are not changed.
22.	k_{22}	A. increased 10 times. B. decreased 10 times.	Ras activation becomes faster for (A) and slower	Ras activation becomes faster for (A) and slower

			for (B). Qualitative features are not changed.	for (B). Qualitative features are not changed.
22.	k_{22}	A. increased 10 times. B. decreased 10 times.	Ras activation becomes slower for (A) and faster for (B). Qualitative features are not changed.	Ras activation becomes slower for (A) and faster for (B). Qualitative features are not changed.
22.	k_{22}^f	A. increased 2 times. B. decreased 2 times. The comments in the last two columns for this parameter are for 2 fold changes. Upon changing the value 10 fold, the region of bistability and hysteresis falls in unrealistic values of species concentrations, but there is no qualitative	Rate of Ras activation increases or decreases for A or B respectively. Qualitative features are not changed. Details in Fig. S16a.	Rate of Ras activation increases or decreases for A or B respectively. Qualitative features are not changed. Details in Fig. S16b.

		change in results.		
23.	k_{23}	A. increased 10 times. B. decreased 10 times.	Hardly any change for (A) or (B). Qualitative features are not changed.	Hardly any change for (A) or (B). Qualitative features are not changed.
24.	k_{24}	A. increased 10 times. B. decreased 10 times.	Hardly any change for (A) or (B). Qualitative features are not changed.	Hardly any change for (A) or (B). Qualitative features are not changed.
25.	k_{25}	A. increased 10 times. B. decreased 10 times.	Hardly any change for (A) or (B). Qualitative features are not changed.	Hardly any change for (A) or (B). Qualitative features are not changed.
25.	k_{-25}	A. increased 10 times. B. decreased 10 times.	Hardly any change for (A) or (B). Qualitative features are not changed.	Hardly any change for (A) or (B). Qualitative features are not changed.
26.	k_{26}	A. increased 10 times. B. decreased 10 times.	Ras activation becomes faster for (A) and slower for (B). The bimodal distribution	Ras activation becomes faster for (A) and slower for (B). Qualitative features are

			<p>in Fig. 4a occurs at an earlier time (A) or later time (B). Qualitative features are not changed.</p>	not changed.
26.	k_{26}	<p>A. increased 10 times.</p> <p>B. decreased 10 times.</p>	<p>Ras activation becomes slower for (A) and faster for (B). The bimodal distribution in Fig. 4a occurs at a later time (A) or an earlier time (B). Qualitative features are not changed. Details in Fig. S17a.</p>	<p>Ras activation becomes slower for (A) and faster for (B). Qualitative features are not changed. Details in Fig. S17b.</p>

Table S13: Parameter Sensitivity for the concentrations used for receptor stimulation simulations

All the concentrations are varied 5 times, because a 10 fold variation would imply 10 times change in cell volume or surface area which makes it an unrealistic variation.

Species	Variation	Effect on cell population distributions	
		Low signal	High signal
TCR	A. 5 times increase. B. 5 times decrease.	Hardly any change for both (A) and (B). Qualitative features are not changed.	Hardly any change for both (A) and (B). Qualitative features are not changed.
Lck	A. 5 times increase. B. 5 times decrease.	Very little change for (A) or (B). Qualitative features are not changed.	Very little change for (A) or (B). Qualitative features are not changed.
ZAP70	A. 5 times increase. B. 5 times decrease.	Very little change for (A) or (B). Qualitative features are not changed. Details in Fig. S18a.	Very little change for (A) or (B). Qualitative features are not changed. Details in Fig. S18b.
LAT	A. 5 times increase. B. 5 times decrease.	Very little change for (A) or (B). See Fig. S19a for details. Qualitative features are not changed.	Very little change for (A) or (B). See Fig. S19b for details. Qualitative features are not changed.
Grb2	A. 5 times increase.	Very little change for (A) or	Very little change for (A) or

	B. 5 times decrease.	(B). Qualitative features are not changed. Details in Fig. S20a.	(B). Qualitative features are not changed. Details in Fig. S20b.
PLC γ	A. 5 times increase. B. 5 times decrease.	Very little change for (A) or (B). Qualitative features are not changed.	Very little change for (A) or (B). Qualitative features are not changed.
PIP $_2$	A. 5 times increase. B. 5 times decrease.	Ras activation becomes faster and slower for (A) and (B) respectively. Qualitative features are not changed.	Ras activation becomes faster and slower for (A) and (B) respectively. Qualitative features are not changed.

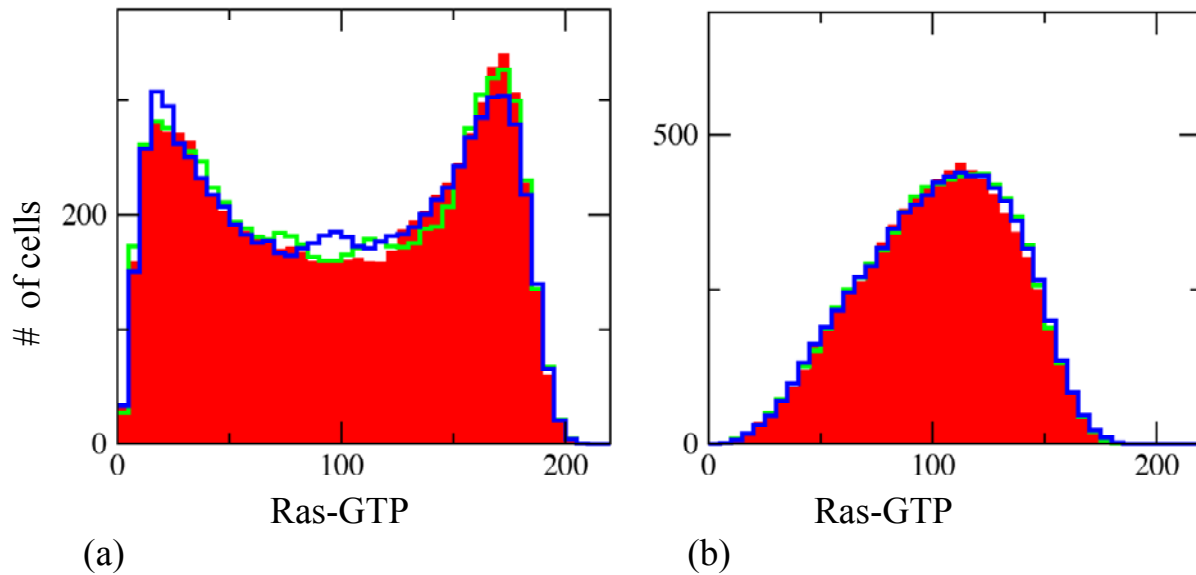


Fig. S13 Variation of TCR-pMHC binding rate (k_{10}): The TCR-pMHC binding (k_{10}) rate is increased (green) and decreased (blue) 10 times and compared with the base case (red histograms) for wild type cells. (a) The distributions shown are for weak stimulation at $t=15$ mins. The bimodal distribution is qualitatively unaffected by the variations. (b) Distributions at $t=7$ mins for strong stimulation.

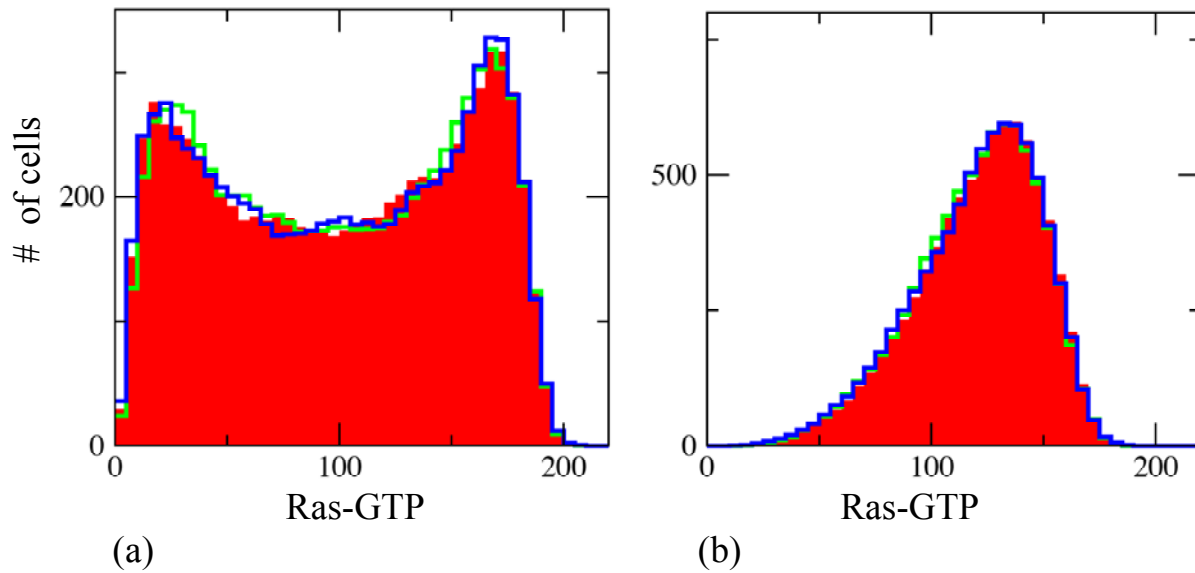


Fig. S14 Variation of LAT unbinding rate (k_{-16}) from pZAP-LAT complexes: The LAT species unbinding (k_{-16}) rate from pZAP-LAT is increased (green) and decreased (blue) 10 times and compared with the base case (red histograms) for wild type cells. (a) Distributions for weak stimulation at $t=15$ mins. (b) Distributions for strong stimulation at $t=7$ mins.

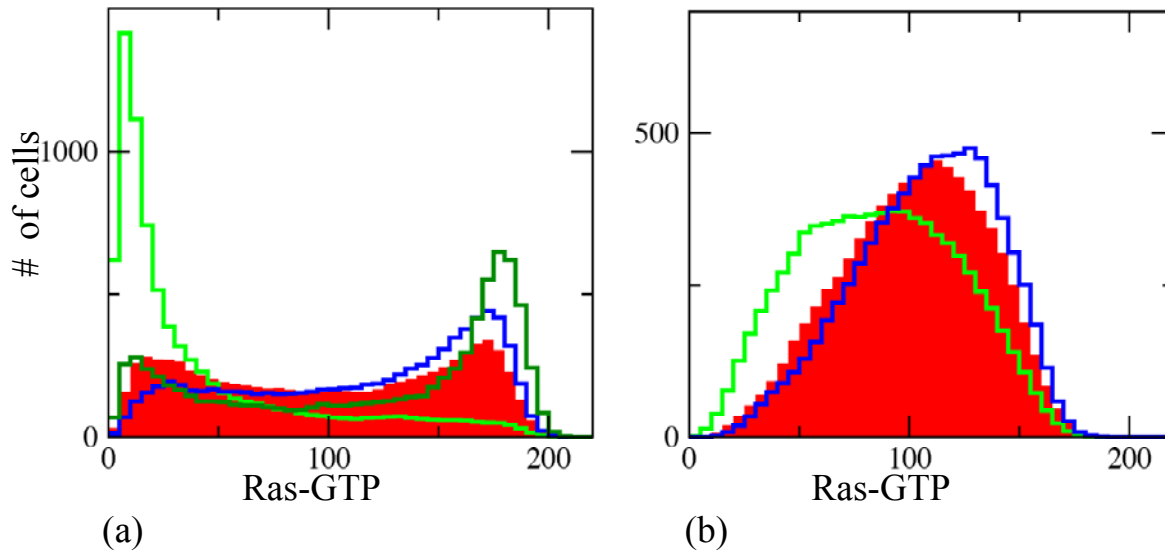


Fig. S15 Variation of PLC γ unbinding rate (k_{-19}) from PLC γ -pLAT complexes:

The unbinding (k_{-19}) rate of PLC γ from PLC γ -pLAT complexes is increased (green) and decreased (blue) 10 times and compared with the base case (red histograms) for wild type cells. (a) Case for weak stimulation at $t=15$ mins. The Ras activation slows down as shown by the green histogram as the unbinding rate is increased, thus, the bimodal distribution in that case occurs at a later time point ($t=20$ mins). (b) Distributions for strong stimulation at $t=7$ mins. They show similar pattern of Ras activation as in (a).

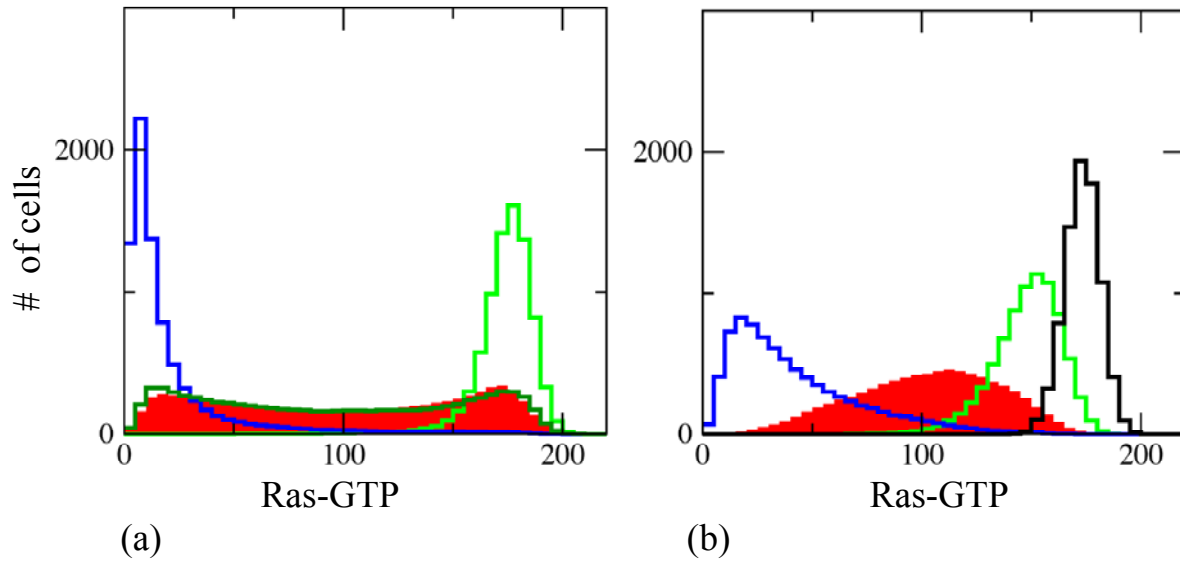


Fig. S16 Variation of DAG production rate (k_{22}^f): The DAG production rate (k_{22}^f) rate is increased (green) and decreased (blue) 2 times and compared with the base case (red histograms) for wild type cells. (a) Distributions shown for weak stimulation at $t=15$ mins. Increasing or decreasing DAG production rate increases and decreases the rate of Ras activation respectively. The bimodal distribution at $t=15$ mins when DAG production rate is increases can be restored (dark green) by decreasing Rasgrp1 concentration 0.75 times. (b) Distributions shown for strong stimulation at $t=7$ mins. The qualitative behavior of rate of Ras activation is similar to (a). When DAG production rate is decreased the robust Ras activation (black) occurs at a later time ($t=20$ mins).

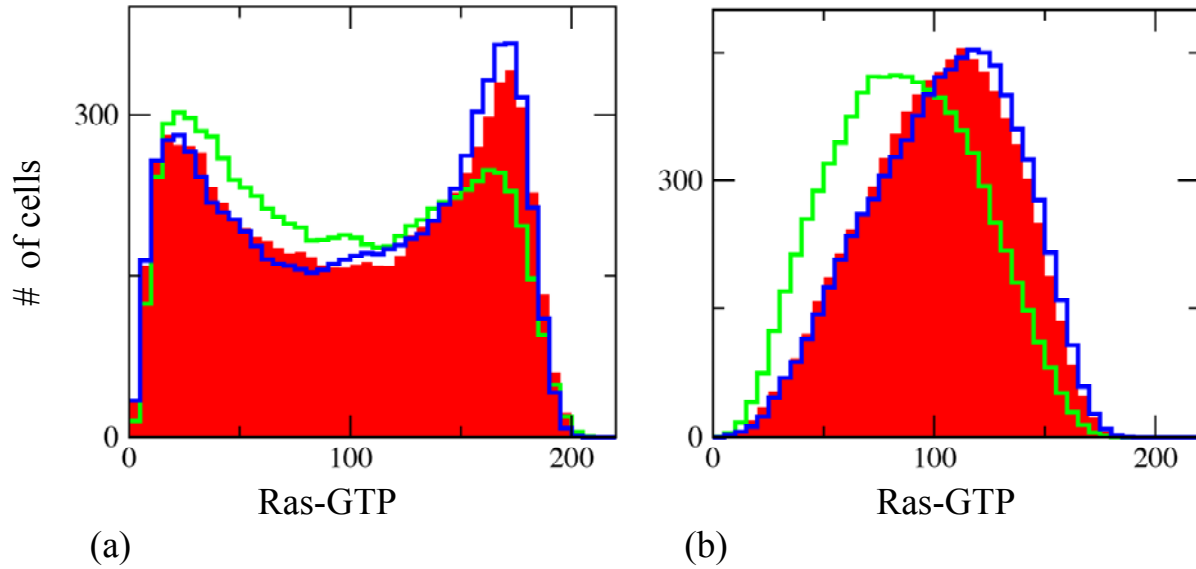


Fig. S17 Variation of unbinding rate (k_{26}) of SOS from Grb2 rate: The unbinding rate (k_{26}) of SOS from Grb2-SOS complexes is increased (green) and decreased (blue) 10 times and compared with the base case (red histograms) for wild type cells. (a) Distributions for weak stimulation. Rate of Ras activation decreases or increases as the unbinding rate k_{26} is increased or decreased respectively. The bimodal distribution at $t=15$ mins for the base case occurs at later time ($t=20$ mins, green) and an earlier time ($t=13$ mins, blue) k_{26} is increased or decreased respectively. (b) All distributions are shown at $t=7$ mins for strong stimulation. Similar qualitative behavior of Ras activation as in (a).

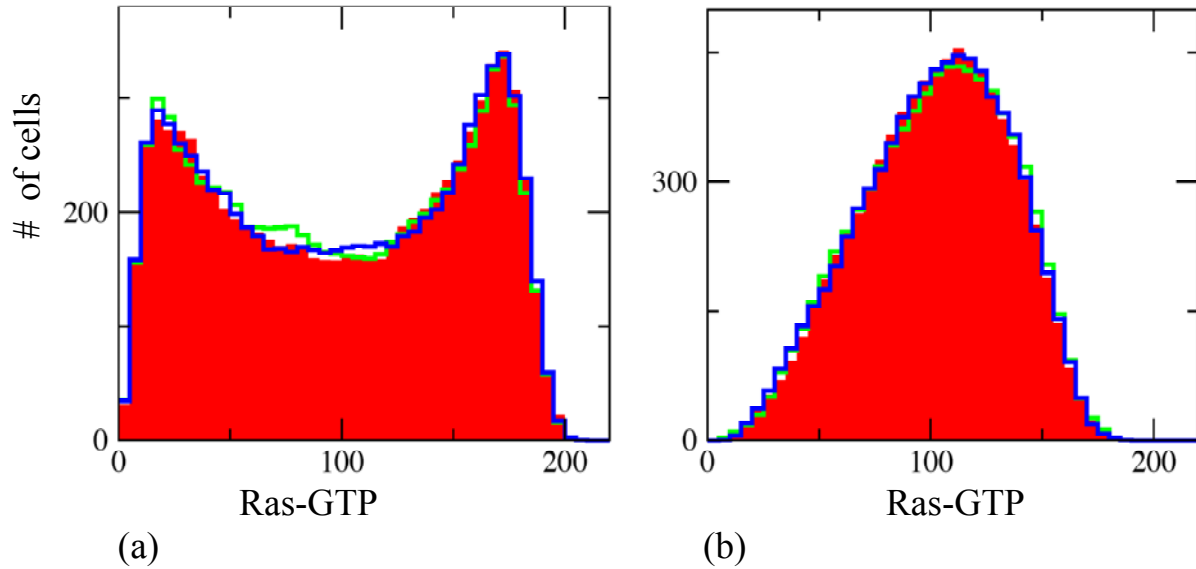


Fig. S18 Variation in ZAP70 concentration: The ZAP70 concentration is increased (green) and decreased (blue) 5 times and compared with the base case (red histograms) for wild type cells. (a) Distributions for weak stimulation at $t=15$ mins. (b) Distributions for strong stimulation at $t=7$ mins.

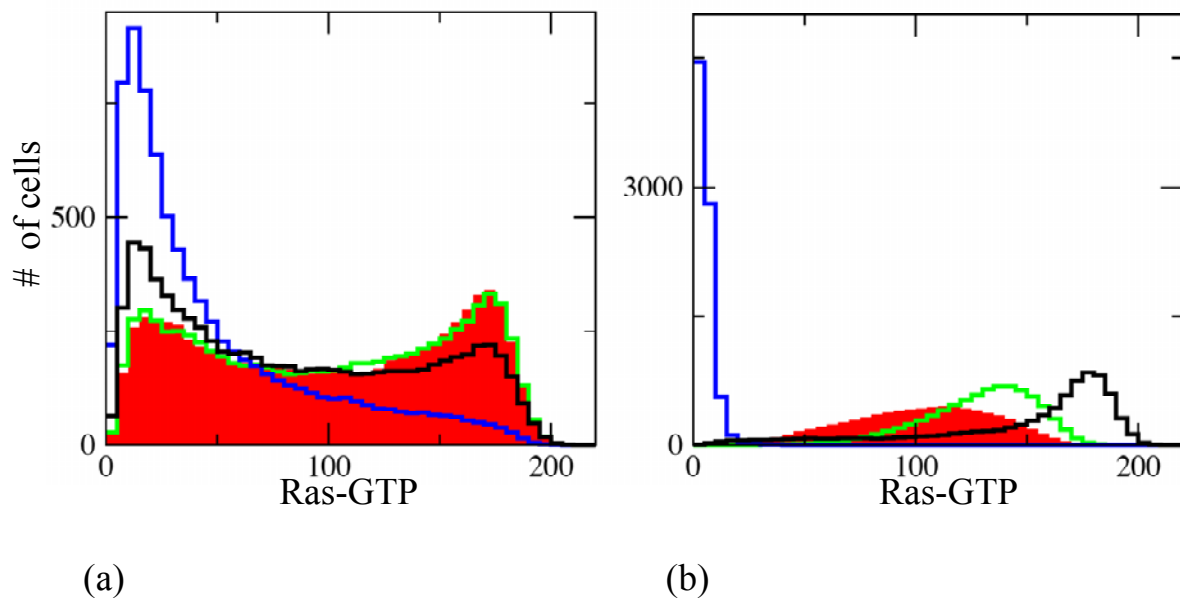


Fig. S19 Variation in LAT concentration: The LAT concentration is increased (green) and decreased (blue) 5 times and compared with the base case (red histograms) for wild type cells. (a) Case for weak stimulation at $t=15$ mins. Rate of Ras activation increases or decreases as LAT

concentration is increased or decreased. When LAT concentration is 5 times lower, the bimodal distribution occurs at a later time point ($t=17$ mins, black). (b) Case for strong stimulation at $t=7$ mins. Similar variation of Ras activation as the LAT concentration changes. The robust Ras stimulation at 5 times less LAT concentration occurs at a later time point ($t=20$ mins, black) than the base case.

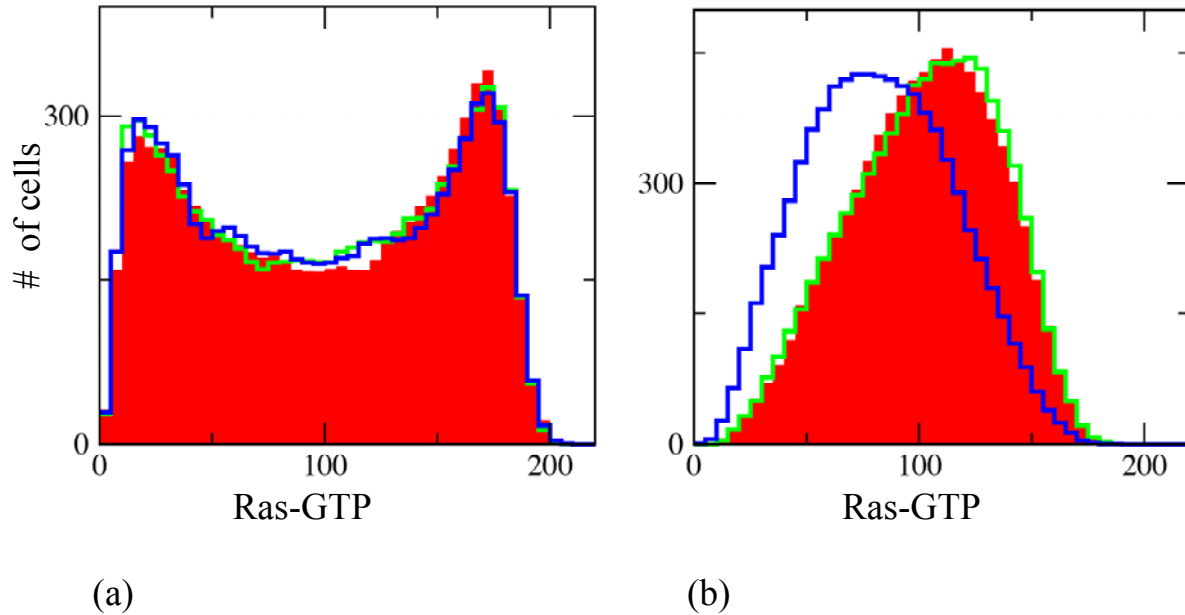


Fig. S20 Variation in Grb2 concentration: The Grb2 concentration is increased (green) and decreased (blue) 5 times and compared with the base case (red histograms) for wild type cells. (a) Distributions for weak stimulation at $t=15$ mins. (b) Distributions for strong stimulation at $t=7$ mins.

Supplemental References.

1. T. Fujisawa *et al.*, *J Biochem (Tokyo)* **115**, 875 (May, 1994).
2. P. H. Lommerse *et al.*, *Biophys J* **91**, 1090 (Aug 1, 2006).
3. H. Sondermann *et al.*, *Cell* **119**, 393 (Oct 29, 2004).
4. T. S. Freedman *et al.*, *Proc Natl Acad Sci U S A* **103**, 16692 (Nov 7, 2006).
5. S. Boykevisch *et al.*, *Curr Biol* **16**, 2173 (Nov 7, 2006).
6. M. R. Ahmadian, U. Hoffmann, R. S. Goody, A. Wittinghofer, *Biochemistry* **36**, 4535 (Apr 15, 1997).
7. P. Gideon *et al.*, *Molecular and Cellular Biology* **12**, 2050 (MAY, 1992).
8. M. Trahey, F. McCormick, *Science* **238**, 542 (OCT 23, 1987).
9. a. Fujioka *et al.*, *Journal of Biological Chemistry* **281**, 8917 (MAR 31, 2006).
10. S. Sasagawa, Y. Ozaki, K. Fujita, S. Kuroda, *Nature Cell Biology* **7**, 365 (APR, 2005).
11. B. Schoeberl, C. Eichler-Jonsson, E. D. Gilles, G. Muller, *Nat Biotechnol* **20**, 370 (Apr, 2002).
12. U. S. Bhalla, R. Iyengar, *Science* **283**, 381 (JAN 15, 1999).
13. B. N. Kholodenko, O. V. Demin, G. Moehren, J. B. Hoek, *J Biol Chem* **274**, 30169 (Oct 15, 1999).
14. N. G. v. Kampen, *Stochastic processes in physics and chemistry*, North-Holland personal library. (North-Holland, Amsterdam; New York, ed. Rev. and enl., 1992), pp. xiv, 465 p.
15. D. T. Gillespie, *Journal of Physical Chemistry* **81**, 2340 (1977).
16. H. H. McAdams, A. Arkin, *Proc Natl Acad Sci U S A* **94**, 814 (Feb 4, 1997).
17. a. B. Bortz, M. H. Kalos, J. L. Lebowitz, *Journal of Computational Physics* **17**, 10 (1975).
18. K. Saito, E. Ito, Y. Takakuwa, M. Tamura, M. Kinjo, *FEBS Lett* **541**, 126 (Apr 24, 2003).
19. C. Lenzen, R. H. Cool, H. Prinz, J. Kuhlmann, A. Wittinghofer, *Biochemistry* **37**, 7420 (MAY 19, 1998).
20. Q. J. Li *et al.*, *Nat Immunol* **5**, 791 (Aug, 2004).
21. S. M. Alam *et al.*, *Immunity* **10**, 227 (Feb, 1999).
22. G. Altan-Bonnet, R. N. Germain, *PLoS Biol* **3**, e356 (Nov, 2005).
23. J. C. Houtman *et al.*, *Biochemistry* **43**, 4170 (Apr 13, 2004).
24. Y. M. Chook, G. D. Gish, C. M. Kay, E. F. Pai, T. Pawson, *Journal of Biological Chemistry* **271**, 30472 (NOV 29, 1996).

Section IV. Cell biological procedures

Cell lines, stimulations, inhibitors, plasmids, and transfections

Human Jurkat leukemic T cells, chicken DT40 B cell lines, and derived lines were generated and cultured as described before (Oh-hora et al., 2003; Roose et al., 2005). Cells were rested for 30 minutes in PBS at 37 °C, or preloaded for 30 minutes with the MEK1/2 inhibitor U0126 at 10 μM (Cell Signaling) or DMSO as control. Stimulations were carried out in PBS at 37 °C with the indicated doses of PMA, C305 supernatant recognizing TCRβ, or M4 antibody recognizing the BCR on DT40 cells, or stimulated with ConA followed by α-MM treatment (Weiss et al., 1987). Plasmids were described before (Boykevisch et al., 2006; Roose et al., 2005; Roose et al., 2007). Jurkat and derived cell lines were transfected as described before (Roose et al., 2005). In short, 20 x 10⁶ cells in 0.3 ml of RPMI, 10% FCS, glutamine, without Pen/Strep were transfected by electroporation using a Biorad electroporator (Biorad) set at 250 mV, 960μF.

Western blot analysis

Expression levels of various proteins were determined and quantitated by Western blot analysis of 1% NP40 lysates as described before (Roose et al., 2005). In short, cell equivalents were analyzed per sample using the following antibodies: RasGRP1 (A176), Phospho-MEK1/2 (Ser217/221), Phospho-p44/42 MAP Kinase (Thr204/Tyr204), Myc-tag (9B11) (Cell Signaling), α-tubulin (Sigma), Ras (Upstate Biotechnologies) for detection of Human Ras, and Pan-Ras (Calbiochem) for detection of chicken Ras. Proteins were visualized using Western Lightning chemiluminescence reagent plus (Perkin Elmer) and a Kodak Image Station 440CF and Kodak ID Image Analysis Software 3.5 to quantify expression levels.

Intracellular FACS staining for P-ERK

FACS assays were carried out as described before (Roose et al., 2005) using APC-conjugated CD69 or CD16 (BD Biosciences). Intracellular FACS stainings for ERK phosphorylation were performed using Phospho-p44/42 MAP Kinase (Thr204/Tyr204) antibody (Cell Signaling). Cells were seeded

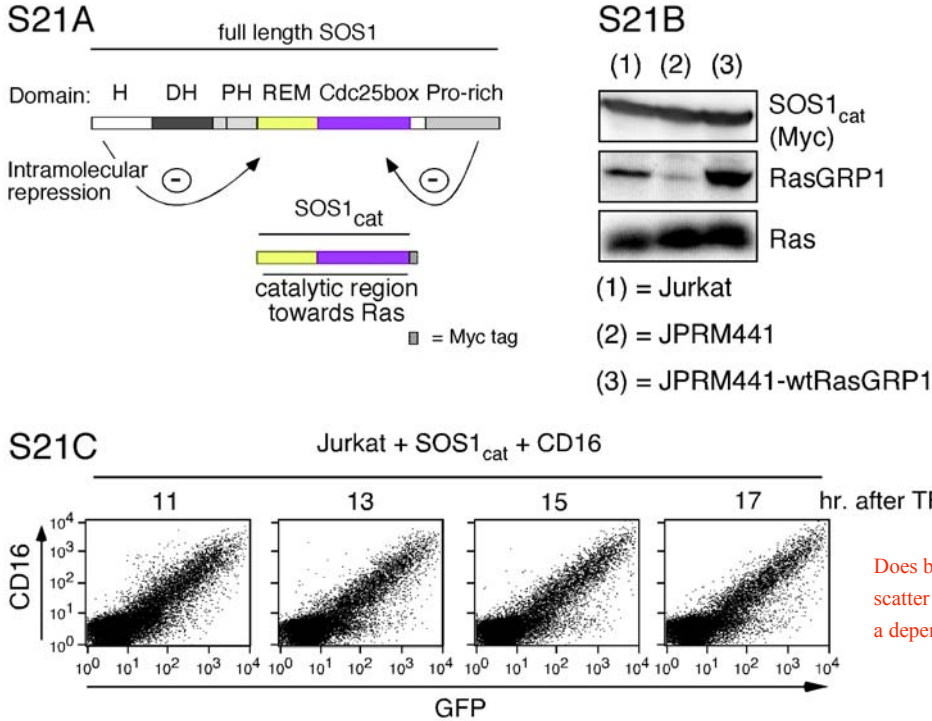
in round bottom 96 well plates at 2.0×10^6 cells/75 μ l (per well). Cells were stimulated with 75 μ l of 2x stimulation mix and subsequently fixed for 20 minutes with 150 μ l fixation buffer (Cytofix/Cytoperm, BD Biosciences). Cells were washed twice in staining buffer (SB; Ca/Mg free PBS, 2 mM EDTA, 1% BSA) and permeabilized for 30 minutes on ice by drop-wise addition of 200 μ l 90% methanol (at -20°C) to a loosened cell pellet. Half of the sample was washed 3 times in SB and stained for 45 minutes at RT in 50 μ l SB containing 1 μ l Phospho-p44/42 MAP Kinase antibody and 1 μ l normal goat serum (NGS) (Jackson Immunoresearch Laboratories). Subsequently, cells were washed 2 times in SB and stained for 45 minutes at RT in the dark with 50 μ l SB containing 1 μ l normal goat serum and 1 μ l PE- or APC-conjugated AffiniPure F(ab')₂ fragment Donkey Anti-Rabbit IgG (Jackson Immunoresearch Laboratories), washed 3 times in SB and directly analyzed by FACS.

For primary T cells, lymph nodes were extracted and single cell suspensions of these were rested for 30 minutes in RPMI at 37°C in 5% CO₂ (tissue culture incubator). Cells were subsequently stimulated with 25 $\mu\text{g/ml}$ (WEAK) or 125 $\mu\text{g/ml}$ (STRONG) 2C11 antibody (Harlan) and 50 $\mu\text{g/ml}$ crosslinking goat-anti-armerian hamster secondary antibody (Jackson Immuno research). Alternatively LN T cells were stimulated with 125 ng/ml (WEAK) or 250 ng/ml (STRONG) PMA. To optimize stainings on primary cells, Methanol permeabilized cells were first rehydrated for 20 minutes in SB and subsequently stained as described above. APC-conjugated AffiniPure F(ab')₂ fragment Donkey Anti-Rabbit IgG (Jackson Immunoresearch Laboratories) was combined with cell surface staining for CD4 (anti-CD4-PE) and CD8 (anti-CD8-FITC, both BD Biosciences.)

Ras activation assays

Activation of Ras was analyzed by a RasGTP pull-down assay essentially according to the manufacturer's instructions (Upstate). For hysteresis experiments, 20×10^6 Jurkat T cells or 40×10^6 DT40 B cells were rested in 400 μ l PBS at 37°C and stimulated with 400 μ l 2x stimulation (with 2X PP2 or DMSO) at $t=0$. 600 μ l was injected in 600 μ l ice-cold 2x MLB for pull-downs. 200 μ l was added to 200 μ l 2x NP40 lysis buffer for analysis of whole cell lysates. Alternatively, cells were rested in 320 μ l PBS at 37°C and 320 μ l 2x stimulation was added at $t=0$, followed by 160 μ l 5X PP2 or DMSO at $t=3$. Thus effectively these stimulations were diluted out 1.25 fold (800/640) between minute 3 and 7. We chose for this method rather than

addition of 160 μ l inhibitor mix with stimulating antibody which could possibly cause a second wave of stimulation. Since Src kinase inhibitor PP2 (Calbiochem) was not preloaded but added at $t=0$ or $t=3$ minutes, these experiments required a slightly higher concentrations of PP2 than one would use with preloading the cells. For Jurkat T cells 5, 10, 20, and 40 μ M of PP2 was used and for DT40 B cells 20, 40, 60, 80 μ M of PP2. For ConA serial stimulation experiments, cells were rested in 240 μ l PBS at 37°C and 240 μ l 2x ConA stimulation was added at $t=0$, followed by 10 μ l 50x α -MM at $t=3$ minutes, and 10 μ l 50x α -BCR stimulation at $t=12$ minutes. MLB lysates were tumbled in the coldroom with 15 μ l of RAF-1 RBD agarose for 30 minutes, washed 3 times in ice-cold NP40 lysis buffer after which the agarose was resuspended in sample buffer, boiled, and loaded. The RasGTP pull down presented in the figures represents material from 15×10^6 Jurkat T cells or 30×10^6 DT40 B cells per lane. The total Ras levels was determined analyzing 0.3×10^6 Jurkat T cells or 0.6×10^6 DT40 B cells per lane (1/50th).



Does bimodality show up as a hole in the scatter diagram for an independent variable and a dependent variable?

Fig. S21. SOS1cat expression in wildtype and RasGRP1 deficient Jurkat T cells.

S21A. Cartoon of the protein domains in full length SOS and the intramolecular repression. H = Histone folds, DH/PH = Dbl-homology, Pleckstrin-homology domain, REM = Ras exchange motif, Cdc25 = Cdc25 homology domain, Pro-rich = Proline-rich domain. The REM and Cdc25 box together make up SOS1cat. Both the N-terminal and C-terminal domains inhibit SOS' catalytic activity.

S21B. Analysis of protein expression from the transfections presented in Figures 2C and 3A. Ten µg of Myc-tagged SOS1cat expressing plasmid was cotransfected with ten µg of GFP expressing plasmid in the wildtype Jurkat (1), RasGRP1 deficient JPRM441 (2), and RasGRP1 reconstituted JPRM441 cell lines (3).

S21C. Ten µg of SOS1cat expressing plasmid was cotransfected with ten µg of a chimeric CD16/CD7 expression construct and GFP expressing plasmid in the wildtype Jurkat. Transfected cells were analyzed for CD16 (using anti-CD16-APC) and GFP expression as before at various time points after transfection. Note the absence of a bimodal pattern for CD16. In addition, note the strong linear correlation between GFP and CD16 expression driven of separate plasmids in the same transfection.

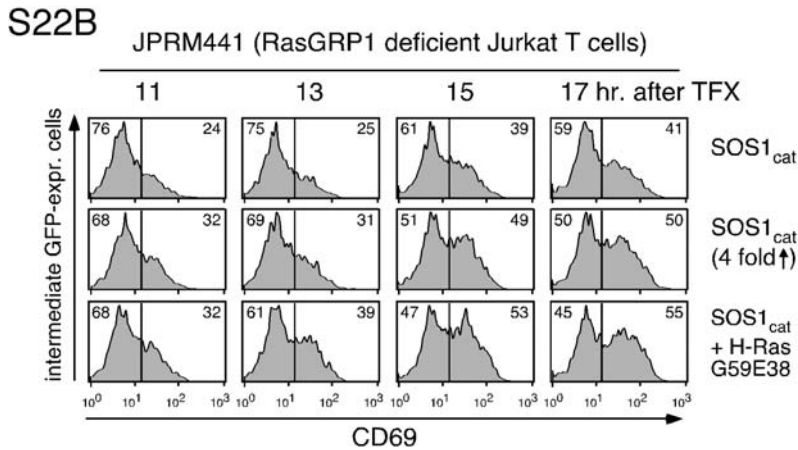
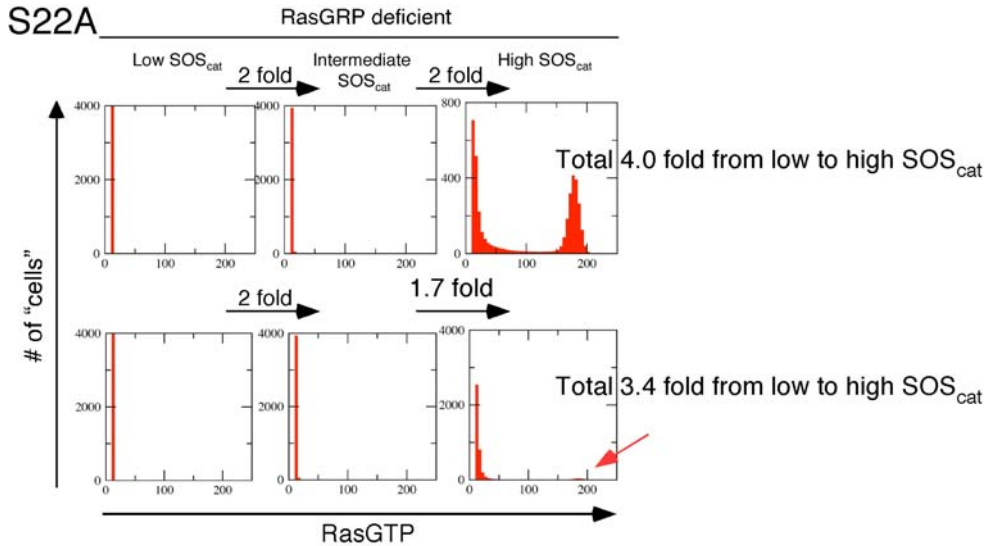


Fig. S22. RasGRP deficiency results in a relative block of $SOS1_{cat}$ -induced bimodal signals.

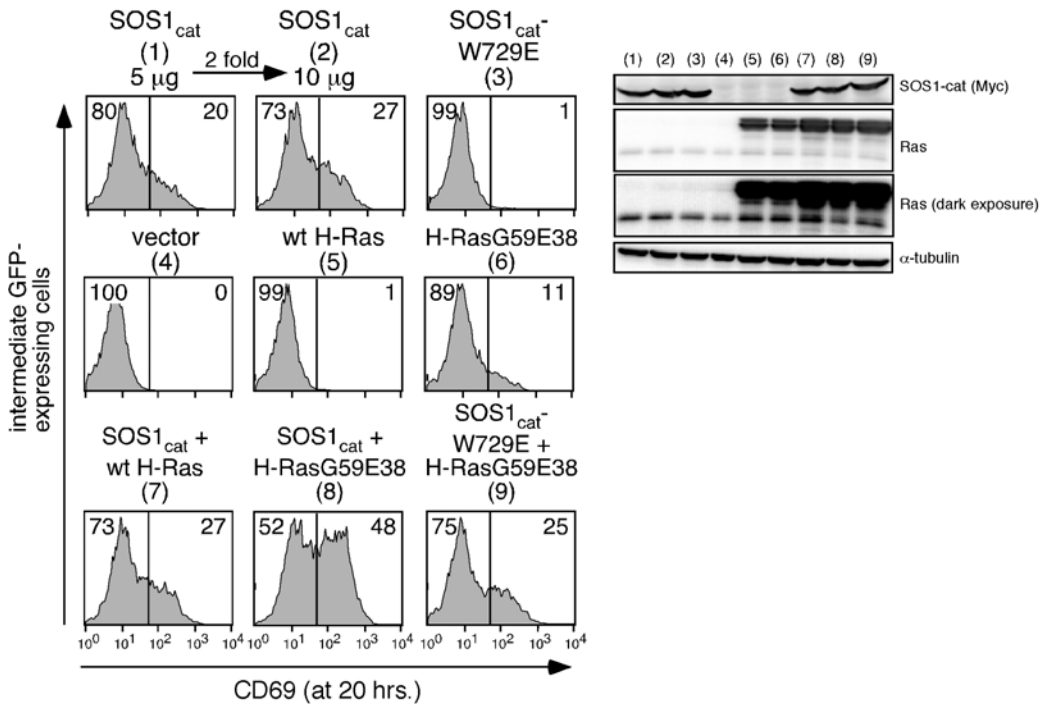
S22A. Distribution of Ras-GTP histograms in a RasGRP deficient cell population calculated from our stochastic simulations at low, intermediate, or high levels of SOS_{cat} . Note the difference in patterns by increasing SOS_{cat} 4.0 fold versus 3.4 fold, demonstrating the relative impairment of SOS_{cat} signaling in a RasGRP deficient state as well as the subtle amount of "cells" with high RasGTP in the bottom right histogram. For a complete description of the Gillespie-based mathematical model, see Supplement, Section II (Tables S4-S8, Figures S5-S12).

S22B. RasGRP1 deficient JPRM441 were transfected with either 15 or 60 μ g $SOS1_{cat}$ (4 fold increase) or, in the third row, with 15 μ g $SOS1_{cat}$ with 2 μ g H-RasG59E38, together with 10 μ g GFP and empty vector to a total amount of 70 μ g DNA. Induction of CD69 was analyzed over time after transfection in GFP intermediate expressing cells. Numbers indicate the percentages of cells on either side of the divider. S22B is an example of two independent experiments. Note that the impaired ability of $SOS1_{cat}$ to signal in RasGRP1 deficient cells is relative, not absolute.

Das et al., Supplemental figure S22

S23

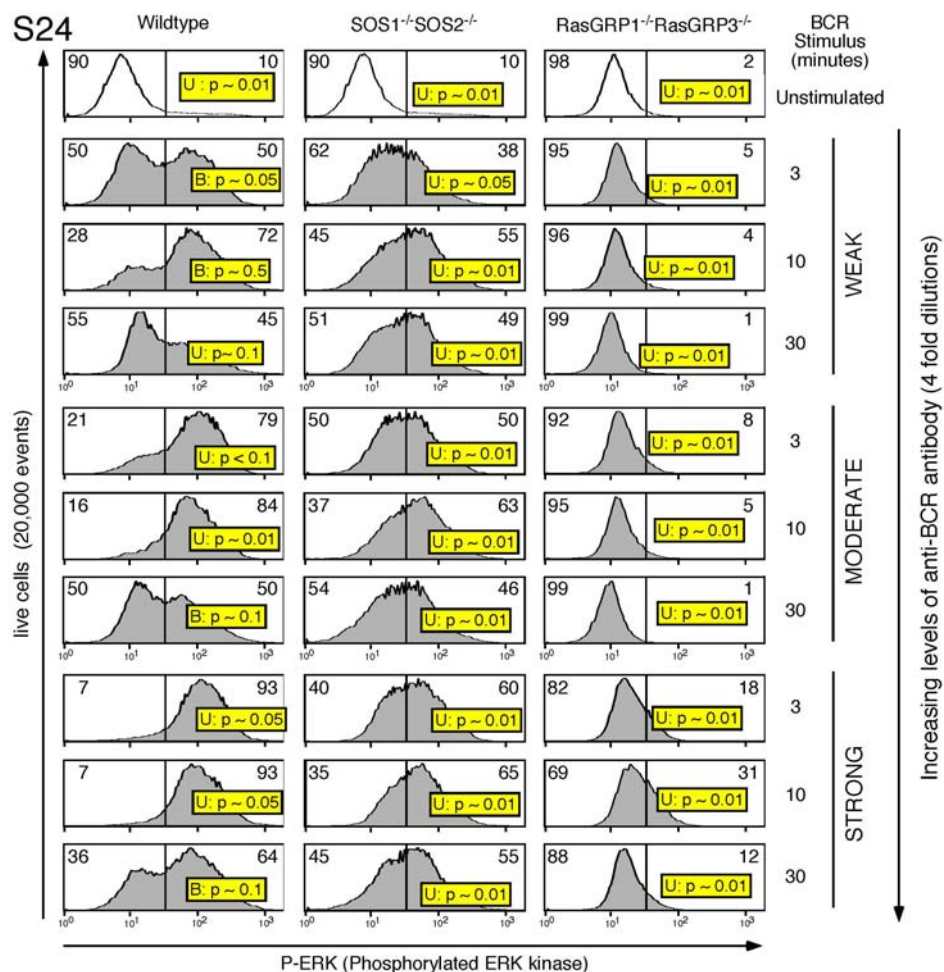
all in JPRM441



S23. Priming of the allosteric pocket in SOS1_{cat} with H-RasG59E38 overcomes RasGRP1 deficiency.

Additional experimental data to the presented figure 3C. RasGRP1 deficient JPRM441 cells were transiently transfected with 10 μ g of GFP and the indicated expression constructs: (1) 5 μ g of SOS1_{cat}, (2) 10 μ g of SOS1_{cat}, (3) 10 μ g of SOS1_{cat}-W729E, (4) empty vector, (5) 2 μ g of wt H-Ras, (6) 2 μ g of H-RasG59E38 ("Ras enhancer"), (7) 5 μ g of SOS1_{cat} plus 2 μ g of wt H-Ras, (8) 5 μ g of SOS1_{cat} plus 2 μ g of H-RasG59E38, (9) 10 μ g of SOS1_{cat}-W729E plus 2 μ g of H-RasG59E38. All transfections contained a total of 22 μ g of DNA by using empty vector as a stuffer. Twenty hours later GFP and CD69 expression was determined. As in Fig. 2C and 3A, intermediate GFP expressing cells were electronically gated for and analyzed for CD69 expression depicted as histograms. Numbers indicate the percentages of cells on either side of the divider. NP40 whole cell lysates were prepared 20 hours after transfection and analyzed for expression of SOS1_{cat} (Myc tagged), Ras (endogenous and overexpressed), and α -tubulin (loading control) proteins.

Das et al., Supplemental figure S23



Geometric mean of P-ERK signal (% of max)
of the total population of DT40 cells

wildtype				SOS1 ^{-/-} SOS2 ^{-/-}				GRP1 ^{-/-} GRP3 ^{-/-}				minutes
0	3	10	30	0	3	10	30	0	3	10	30	
9	30	54	31	10	22	33	28	10	13	13	10	WEAK
9	68	68	33	10	30	42	26	12	15	13	9	MODERATE
9	100	94	48	10	39	43	32	11	19	25	17	STRONG

BCR stimulus

Das et al., Supplemental figure S24

Fig. S24. Digital BCR induced Ras-ERK activation requires SOS.

FACS analysis of ERK phosphorylation in 20,000 individual cells per histogram. The indicated DT40 B cell lines were stimulated with 1:8,000 (WEAK), 1:2,000 (MODERATE) or 1:500 (STRONG) dilutions of BCR stimulating M4 antibody for

3, 10, or 30 minutes, or left unstimulated. Cells were fixed and permeabilized and stained for ERK phosphorylation. P-ERK levels in 20,000 live cells were plotted as histograms. Numbers in histograms represent the percentage of cells on either side of the divider. Numbers in the table represent the geometric mean of PE-fluorescent signal for P-ERK in the complete population of a given sample. Note that similar values at this population level (e.g. five population between 30-33%) are the result of the combined input of very different P-ERK patterns in the histogram made up of all individual cells in a given sample. Yellow boxes indicate Unimodality (U) or Bimodality (B) with their statistical p-value as determined by the Hartigan's test.

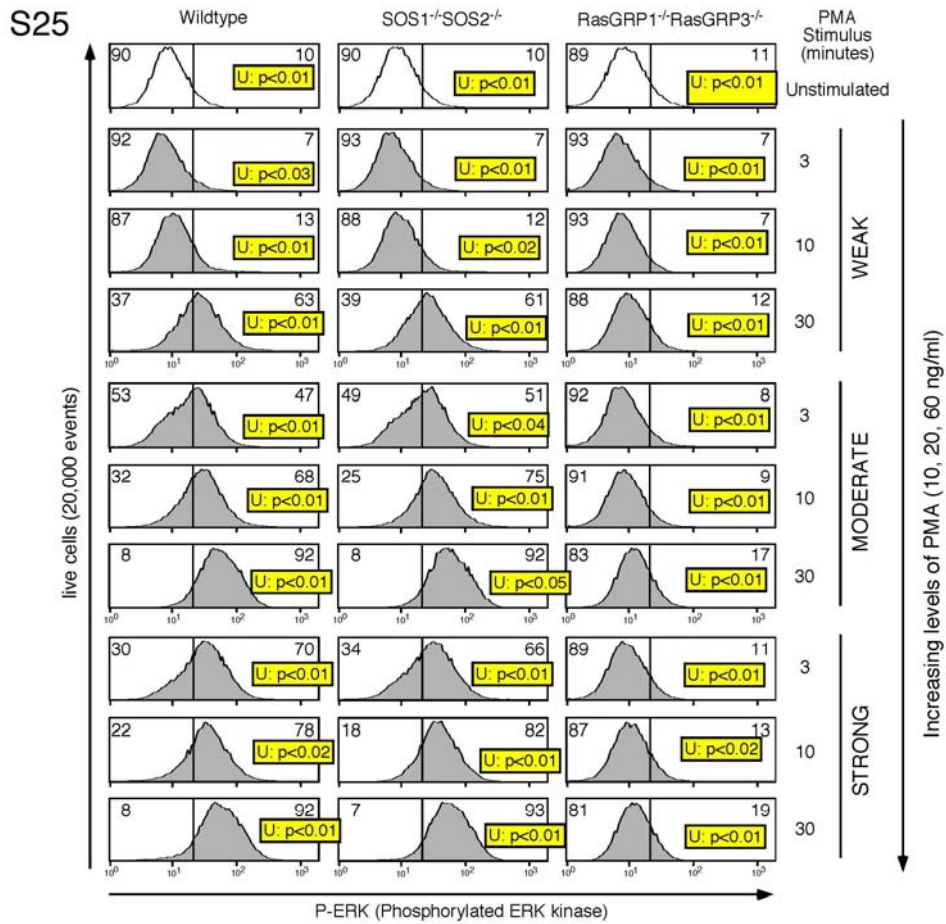
Hartigan's DIP test

We use Hartigan's DIP test (Hartigan and Hartigan, 1985) to determine the unimodality or bi-modality of the FACS data shown in Fig. 2C, 3A,C and Fig. 5. This method has been used by various labs (Batada et al., 2006; Priebe et al., 2004) in recent years. The MATLAB codes used for this test are taken from, <http://www.nicprice.net/diptest/>. Histograms were divided into 120 equal gates going up in signal intensity for P-ERK. For each of these gates the mean fluorescent signal was calculated and the number of number of cells within the gate was determined. These parameters were entered into the Hartigan's test. The original FACS data are averaged over so that a bin interval of 8 bins (intervals of 6 and 10 bins were used for the data in the 3rd panel of Fig. 5E and the 6th panel of 5F respectively) for in the original data corresponds to a single bin in the averaged data set on which the dip test was carried out. This averaging is performed to exclude fluctuations in the data occurring across small variations of intensity in the experiments.

Batada, N. N., Reguly, T., Breitkreutz, A., Boucher, L., Breitkreutz, B. J., Hurst, L. D., and Tyers, M. (2006). Stratus not altocumulus: A new view of the yeast protein interaction network. *Plos Biology* 4, 1720-1731.

Hartigan, J. a., and Hartigan, P. M. (1985). The Dip Test of Unimodality. *Annals of Statistics* 13, 70-84.

Priebe, N. J., Mechler, F., Carandini, M., and Ferster, D. (2004). The contribution of spike threshold to the dichotomy of cortical simple and complex cells. *Nature Neuroscience* 7, 1113-1122.



Geometric mean of P-ERK signal (% of max) of the total population of DT40 cells

wildtype				$SOS1^{-/-}SOS2^{-/-}$				$GRP1^{-/-}GRP3^{-/-}$				minutes	PMA stimulus
0	3	10	30	0	3	10	30	0	3	10	30		
16	14	19	46	16	13	17	45	16	13	14	18	WEAK (10 ng/ml)	PMA stimulus
16	32	50	95	16	36	57	98	16	14	15	21	MODERATE (20 ng/ml)	
16	53	61	100	16	49	67	100	16	16	18	24	STRONG (60 ng/ml)	

Fig. S25. Analog PMA induced Ras-ERK activation requires RasGRP.

FACS analysis of ERK phosphorylation analogous to figure S24. Here cells were stimulated with the DAG analog, PMA; either at WEAK (10 ng/ml), MODERATE (20 ng/ml), or STRONG levels (60 ng/ml). Note the absence of a bimodal response.

S26

Transfected Jurkat T cell line

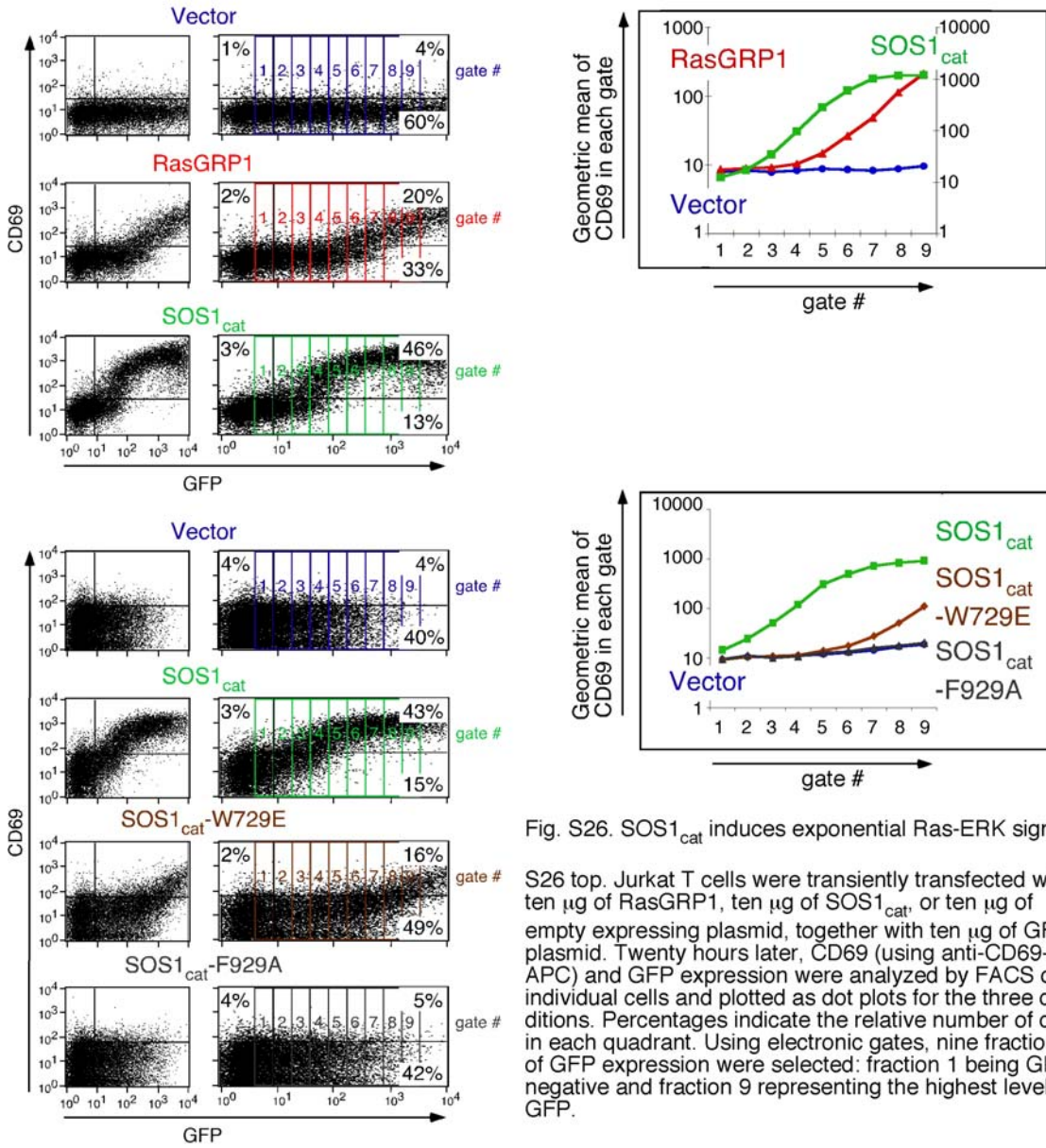


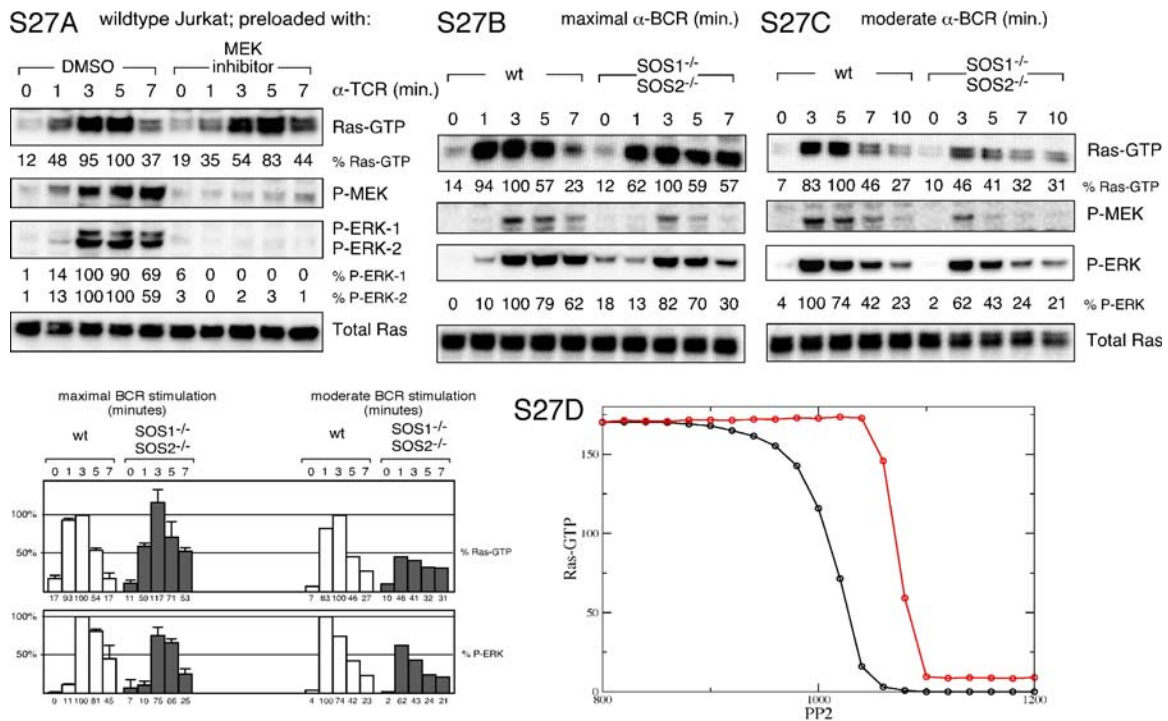
Fig. S26. SOS1_{cat} induces exponential Ras-ERK signals.

S26 top. Jurkat T cells were transiently transfected with ten μ g of RasGRP1, ten μ g of SOS1_{cat}, or ten μ g of empty expressing plasmid, together with ten μ g of GFP plasmid. Twenty hours later, CD69 (using anti-CD69-APC) and GFP expression were analyzed by FACS on individual cells and plotted as dot plots for the three conditions. Percentages indicate the relative number of cells in each quadrant. Using electronic gates, nine fractions of GFP expression were selected: fraction 1 being GFP-negative and fraction 9 representing the highest level of GFP.

The geometric mean of APC fluorescent signal for CD69 was determined in the 9 fractions and plotted for the three conditions on a 10log-scale graph. The left scale on the Y-axis applies to Vector and RasGRP1, the right scale to SOS1_{cat}.

S26 bottom. Analogous to the experiments depicted on the top, introduction of ten μ g of SOS1_{cat} was compared to the same amount of SOS1_{cat}-W729E (in brown, allosteric pocket mutant), SOS1_{cat}-F929A (in grey, GEF pocket mutant), or Vector (in blue). S26 is a representative example of three independent experiments.

Das et al., Supplemental figure S26



Das et al., Supplemental figure S27

Fig. S27. Kinetics of RasGTP induction in untreated versus MEK inhibitor-treated Jurkat T cells, wildtype and SOS1^{-/-}/SOS2^{-/-} DT40 B cells.

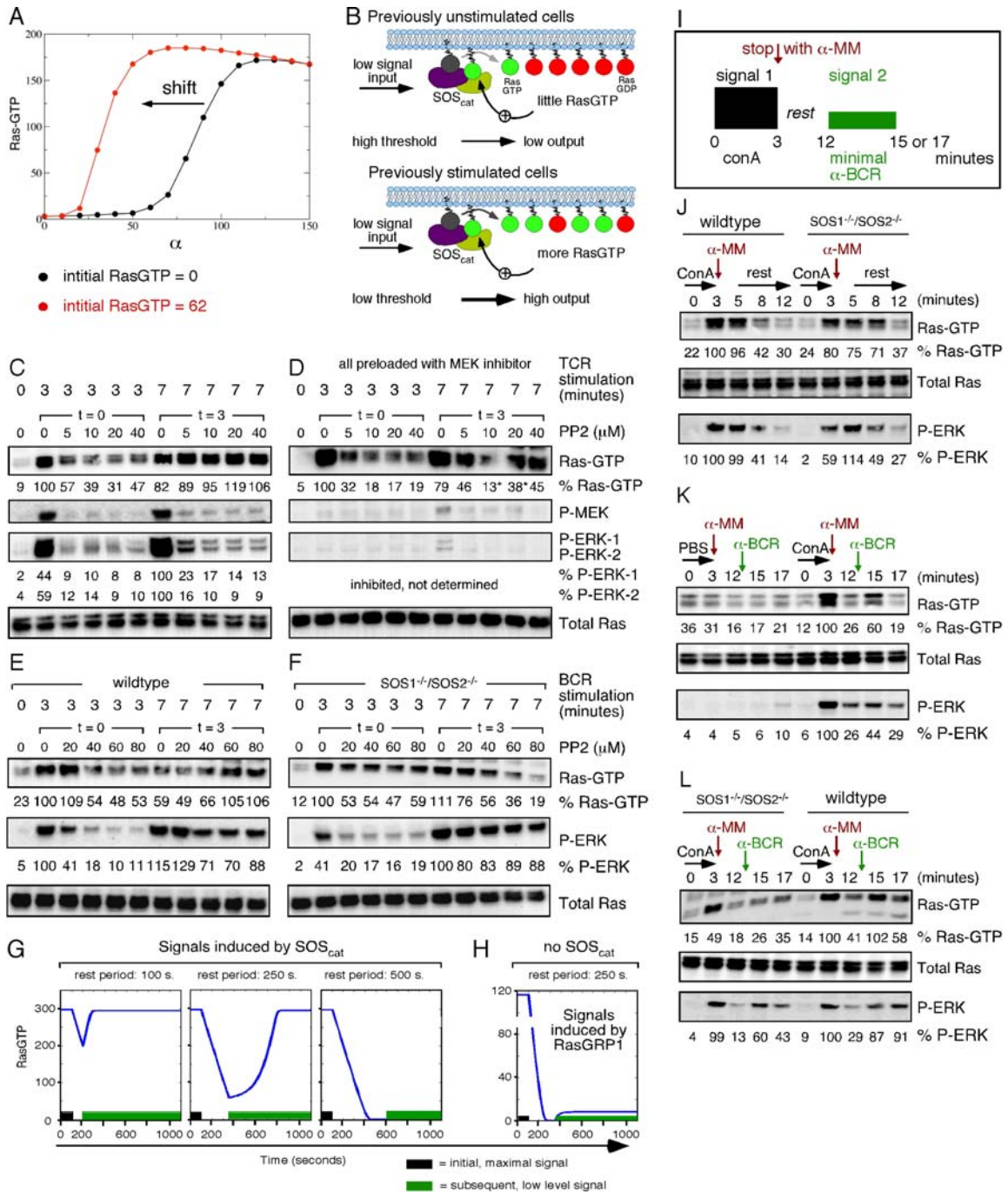
S27A. Ras activation in TCR stimulated Jurkat T cells that were preloaded with DMSO as control or with the MEK1/2 inhibitor U-0126. U-0126 effectively blocks MEK and ERK phosphorylation.

S27B. The kinetics of BCR induced Ras activation in DT40 B cells were determined to design the optimal experiment to test hysteresis in Figure 6E and 6F. Wildtype and SOS1^{-/-}/SOS2^{-/-} DT40 B cells were stimulated for the indicated time intervals with 1:300 diluted M4 (maximal dose). Note that this dose of M4 generates maximal RasGTP levels in both lines at 3 minutes, albeit with somewhat delayed kinetics in SOS1^{-/-}/SOS2^{-/-} cells.

S27C. A moderate dose of M4 (1:1,200) clearly reveals a defect at the level of RasGTP induction in the SOS1^{-/-}/SOS2^{-/-} DT40 B cells. S27B is a representative example of three independent experiments, the mean and standard error for these three experiments is plotted in the bar graph below. Of note, DT40 B cells express only chicken ERK2. The experiment presented in S27C was performed twice.

S27D. Results for hysteresis from simulations with the inhibitor PP2:

The black points (case I) show the RasGTP concentrations at t=12 mins when antigen dose and PP2 are added in the system at t=0. The red points (case II) show the RasGTP concentrations at t=12 mins, when the same amount of antigen dose as in case I is added at t=0, but, PP2 is added at t=6 mins. We see hysteresis for a range of PP2 concentrations. In the simulation, molecules of PP2 bind to molecules of free Lck or Lck bound to the TCR complex. When PP2 is bound to Lck, Lck loses its ability to activate TCR or ZAP. In our model, when Lck, bound to a TCR complex, binds to PP2, the entire complex dissociates (e.g., $\text{TCR}^*-\text{Lck}-\text{pMHC}-\text{ZAP}^*+\text{PP2} \rightarrow \text{TCR} + \text{pMHC} + \text{ZAP} + \text{Lck}-\text{PP2}$) with a rate ($\sim 10 \text{ s}^{-1}$), this process is an abstraction of the collection of processes where, individual activated members of a complex which are essential to be in the activated states to keep the complex intact, get deactivated by various phosphatases, and do not get further activated by the Lck because it is bound to PP2, resulting in the disassociation of the entire complex. For case II, we have some residual Ras activation at large PP2, because, in this case, at the time PP2 is added, the system has already produced some DAG molecules, and those DAG molecules recruit RasGRP1 to the plasma membrane which continue activating low amounts of Ras-GTP, this is an artifact of the model, because, in lymphocytes, DAG kinases will de-activate this pool of DAG which is missing in this model. This is done to keep the numbers of species and reactions manageable in the model without sacrificing any qualitative changes in the results.



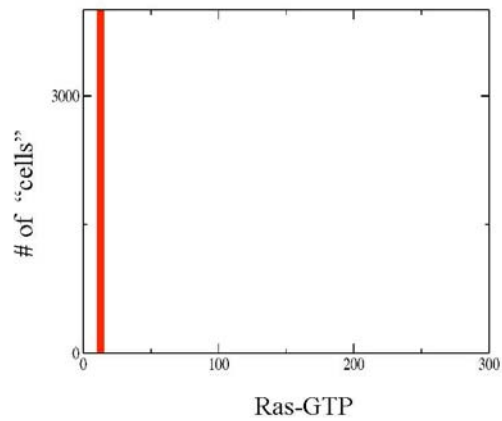
Das et al., Supplemental figure S28

Fig. S28. Hysteresis at the level of RasGTP depends on SOS.

This is the same figure as presented in Figure 6. Here western blot analyses of ERK and MEK phosphorylation (in C-F and J-L) are included. Phospho-ERK and phospho-MEK intensities were determined as described before.

RasGRP deficient
+ H-RasG59E38

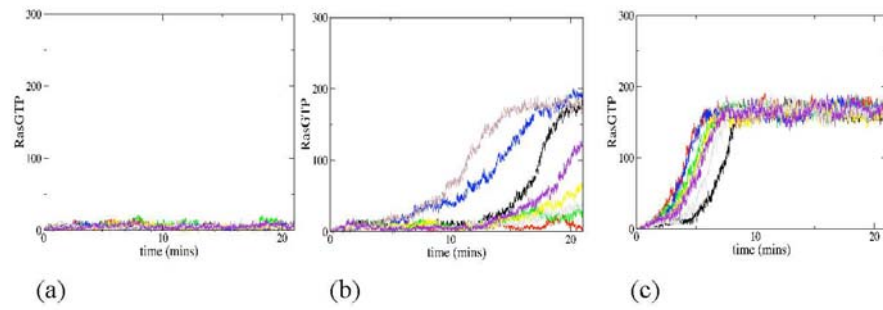
S29



Das et al., Supplemental figure S29

Fig. S29. Bimodality is absent when the positive feedback to SOS is abrogated. The bimodality in Fig. 3D in the main text disappears when the allosteric site is mutated such that it cannot bind to RasGDP or RasGTP. The rest of the parameters used are identical to that of used in Fig. 3D.

S30



Das et al., Supplemental figure S30

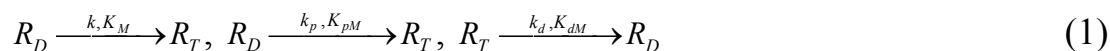
Fig. S30. Trajectories from the stochastic simulation. Representative trajectories are shown (in 8 different colors) from the simulations that correspond to Fig. 2B for (a) low, (b) intermediate and (c) high SOS_{cat} concentrations.

Section VI. Understanding design principles underlying bistable Ras activation through minimal models

Our results showed that the positive feedback in Ras activation mediated through SOS can give rise to bistability in Ras activation (Fig. 1). Here we analyze what are the key ingredients in the dynamics of Ras activation that can lead to emergence of multiple steady states in the system. This study helped uncover the design principles underlying the bistable Ras activation network. Our results (Fig. 1E) also show the interesting interplay between the RasGRP and SOS pathways that enables efficient digital signaling in lymphocyte for a certain range of RasGTP activity and expression. To determine the minimal model required for bistable Ras activation, we start with the model we have determined to contain the necessary ingredients. We then show, various simplifications to this model abrogate bistability. We consider a simple reaction network described in terms of only activated and deactivated forms of Ras. The activation of Ras occurs through two types of enzymes, E and S. The activation mediated by the first enzyme does not involve any positive feedback; thus, E can represent enzymes such as, catalytic sites of SOS molecules with empty or Ras-GDP bound allosteric sites, or the other GEF Rasgrp1. The enzyme, S, describes the enzyme that mediates positive feedback in Ras activation. Thus, S would represent catalytic sites of SOS molecules with Ras-GTP molecules bound to their allosteric sites. Therefore, for simplicity we will assume, concentration of S, $[S] \propto [Ras - GTP]$. The action of the enzymes, E and S are captured in the Michaelis form of activation with constants, $\{k, K_M\}$ and $\{k_p, K_{pM}\}$, respectively. The deactivation of Ras executed by RasGAPs is represented as an enzymatic de-activation of Ras-GTP by an enzyme G. The action of G is described in terms of a Michaelis form with constants, $\{k_d, K_{dM}\}$. The main results of the calculations below are the following, (i) positive feedback regulation of Ras activation; (ii) catalytic activation of Ras through the enzymes S; and (iii) catalytic de-activation of Ras-GTP by G are necessary to have bistability, hysteresis, and digital signaling.

A minimal model:

The model described above can be represented as:



Here, R_D and R_T indicate Ras-GDP and Ras-GTP, respectively. The first reaction describes Ras activation by the enzyme, E and the second reaction describes the positive feedback in Ras activation mediated by SOS molecules bound to Ras-GTP at the allosteric site. The last reaction describes enzymatic de-activation of Ras-GTP by Ras-GAPs (enzyme G). We will assume a Michaelis-Menten form for simplicity. The total number of Ras molecules is conserved, thus, $[R_D] + [R_T] = \beta = \text{const.}$, where, $[X]$ denotes the concentration of species, X. The mean field rate equation for R_T is given by,

$$\frac{d[R_T]}{dt} = \frac{k[E][R_D]}{K_M + [R_D]} + \frac{k_p[R_T][R_D]}{K_{pM} + [R_D]} - \frac{k_d[G][R_T]}{K_{dM} + [R_T]} \quad (2)$$

, where, K_M, K_{pM} and K_{dM} are the Michaelis-Menten constants.

The steady states of Eq. (2) are given by,

$$\begin{aligned} \frac{k[E][R_D]}{K_M + [R_D]} + \frac{k_p[R_T][R_D]}{K_{pM} + [R_D]} - \frac{k_d[G][R_T]}{K_{dM} + [R_T]} &= 0 \\ \Rightarrow \frac{k[E](\beta - [R_T])}{K_M + \beta - [R_T]} + \frac{k_p[R_T](\beta - [R_T])}{K_{pM} + \beta - [R_T]} - \frac{k_d[G][R_T]}{K_{dM} + [R_T]} &= 0 \end{aligned} \quad (3)$$

The above equation gives a fourth order polynomial equation for $[R_T]$. In order to simplify the equation further, we consider the case, $k = 0$, this situation will be relevant when the concentration of Rasgrp1 is zero and concentration of SOS is not very large, so that the production of Ras-GTP through reactions without any positive feedback can be neglected. When, $k = 0$, we get from Eq.(3),

$$\begin{aligned} \frac{k_p[R_T](\beta - [R_T])}{K_{pM} + \beta - [R_T]} - \frac{k_d[G][R_T]}{K_{dM} + [R_T]} &= 0 \\ \Rightarrow k_p x(\beta - x)(K_{dM} + x) - k_d[G]x &= 0 \end{aligned} \quad (4)$$

, where, $x = [R_T]$. To keep the notations simple, from now on we will denote $k_d[G]$ as k_d . From Eq.(4) we get, $x = x_0 = 0$ or,

$$x^2 - (\beta - K_{dM} + k_d/k_p)x + (k_d/k_p)(K_{pM} + \beta) - \beta K_{dM} = 0 \quad (5)$$

which has the following solutions,

$$x_{\pm} = 1/2(\beta - K_{dM} + k_d/k_p) \left[1 \pm \sqrt{1 - \frac{4(k_d/k_p(K_{pM} + \beta) - \beta K_{dM})}{(\beta - K_{dM} + k_d/k_p)^2}} \right] \quad (6)$$

Therefore, if $\beta - K_{dM} + k_d/k_p > 0$, $k_d/k_p(K_{pM} + \beta) - \beta K_{dM} > 0$ and $(\beta - K_{dM} + k_d/k_p)^2 > 4(k_d/k_p(K_{pM} + \beta) - \beta K_{dM})$, both x_+ and x_- are real positive solutions.

Stability: We perform a linear stability analysis of the fixed points $x = \bar{x}^* = \{x_0, x_+, x_-\}$ of Eq. (2) when $k = 0$.

The dynamics described by Eq.(2) can be described as,

$$\frac{dx}{dt} = -\frac{f(x)}{g(x)}$$

, where, $f(x) = k_p x(a_2 x^2 + a_1 x + a_0)$ and $g(x) = (K_{pM} + \beta - x)(K_{dM} + x)$. The coefficients, a_1 , a_2 and a_3 are given by,

$$a_2 = 1$$

$$a_1 = -(\beta - K_{dM} + k_d/k_p)$$

$$a_0 = k_d/k_p(K_{pM} + \beta) - \beta K_{dM}$$

Thus, if $x = \bar{x}^* + \delta\bar{x}$, then, $\frac{d(\delta\bar{x})}{dt} = \bar{Q}(\delta\bar{x})$, where, \bar{Q} is a diagonal matrix with the diagonal elements, $\{q_0, q_+, q_-\}$, shown below,

$$\left\{ q_0 = \frac{1}{g(x_0)} \frac{df}{dx} \Big|_{x=x_0} = -\frac{k_p x_+ x_-}{g(x_0)}, q_+ = \frac{1}{g(x_+)} \frac{df}{dx} \Big|_{x=x_+} = -\frac{k_p x_+(x_+ - x_-)}{g(x_+)}, q_- = \frac{1}{g(x_-)} \frac{df}{dx} \Big|_{x=x_-} = -\frac{k_p x_-(x_- - x_+)}{g(x_-)} \right\}$$

Therefore, when both x_+ and x_- are real positive or complex numbers, the fixed point at $x = x_0 = 0$ is stable, it becomes unstable when one of the fixed points of the pair, x_+ and x_- , is negative. When x_+ and x_- are real positive, then the above analysis shows that the larger fixed point is stable and the other one is unstable.

Now we can try to understand how the fixed points behave as the strength of the positive feedback, k_p , is increased. This will be qualitatively similar to increasing the SOS_{cat} concentration in the system (as in Fig. 1). It will be useful to understand the behavior of the function, $a_1^2 - 4a_0$ for this purpose as k_p is increased. This function is given by,

$$\begin{aligned}
f(y) &= a_1^2 - 4a_0 \\
&= (\beta - K_{dM} + y)^2 - 4(y(K_{pM} + \beta) - \beta K_{dM}) \\
&= (y - y_+)(y - y_-)
\end{aligned}$$

where, $y = k_d/k_p$ and

$$y_{\pm} = (\beta + K_{dM} + 2K_{pM}) \left[1 \pm \sqrt{1 - \frac{(\beta + K_{dM})^2}{(\beta + K_{dM} + 2K_{pM})}} \right]$$

Therefore, when $y_- < y < y_+$, $f(y) < 0$, thus, the solutions in Eq.(6) are complex numbers, only the in the range, $y \leq y_-$ or $y \geq y_+$, x_{\pm} are real.

However, when $y \geq y_+$, x_{\pm} will be greater than β , the total Ras concentration, consequently, the solutions in Eq.(6) will be unphysical. Thus the solutions in Eq.(6) will be physical solutions only when $y \leq y_-$. When, $k_p \rightarrow 0$, $y \rightarrow \infty$, therefore, x_+ and x_- will be unphysical and, $x=0$, will be the only stable fixed point. Thus for small k_p , $x=0$ is a stable fixed point and is the only physical solution. As k_p increases further, the stable and unstable fixed points at non-zero values of x which are physical solutions of Eq.(6) will start appearing when $k_p \geq k_d/y_-$. In this regime, both x_+ and x_- are less than β , and the real positive solutions, $x=0$ and $x=x_+$ correspond to the stable fixed points and $x=x_-$ corresponds to the unstable solution. In this regime the stable fixed point at the higher Ras activation is given by,

$$x_+ = 1/2(\beta - K_{dM} + k_d/k_p) \left[1 + \sqrt{1 - \frac{4(k_d/k_p)(K_{pM} + \beta) - \beta K_{dM}}{(\beta - K_{dM} + k_d/k_p)^2}} \right] \quad (7)$$

Thus, in both these cases the behavior of this system qualitatively represents the fixed point structure shown in Fig. 1C in the main text. Eq.(7) is an approximate analytical formula for the difference between the two stable solutions, or the ‘‘digital jump’’ where SOS targeted to the membrane exceeds a threshold.

When k_p is increased to a very large value (i.e., $k_p > k_d/(\beta K_{dM}(K_{pM} + \beta))$), x_- will become negative, thus, the fixed point at $x=0$ will become unstable and the only stable fixed point will be at $x=x_+$. In this case, the behavior of this system is different (it has an additional unstable fixed point at $x=0$) from the one shown in Fig. 1C. However, this is expected, because in this regime because of the high SOS concentration the production of Ras-GTP without a positive feedback is significant which is not captured in the limit $k=0$. We expect this simple model at a non-zero k will capture the qualitative behavior

of Fig. 1C in this regime. Since having $k \neq 0$ makes the steady state equation a fourth order polynomial equation, it is harder to solve it exactly analytically, but it should yield little more than one stable fixed point for large k_p . The fixed point structure of this simple model for a particular set of parameters is shown in the figure below.

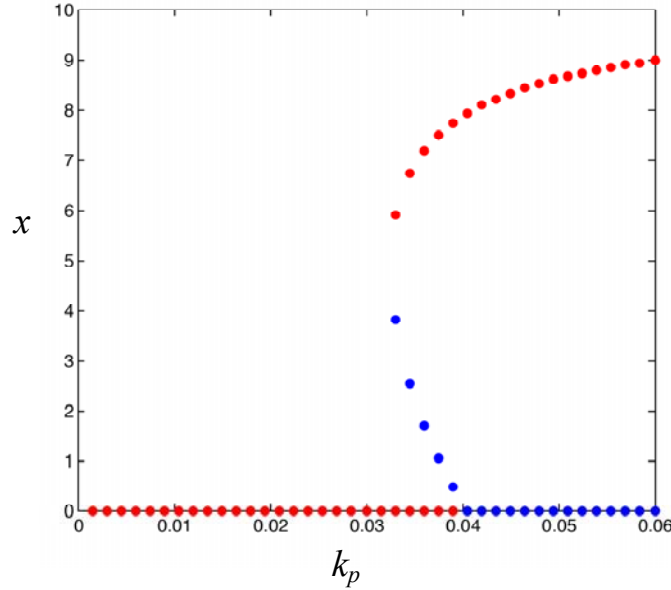


Fig. S31 The stable (red) and unstable (blue) fixed points for the simple model is shown as the strength of the positive feedback, k_p , is varied. The values of the parameters are the following: $\beta = 10$, $K_{pM} = 2.62$, $K_{dM} = 10$, $k = 0$ and $k_d = 10$.

Dependence of the solutions on the parameters:

We can also understand the dependence of the solution in Eq.(7) as the parameters in the system are varied. All the variations here turn out to be consistent with the sensitivity analysis reported in Table S3. (a) An increase in the Ras deactivation catalytic rate, k_d , will result in an increase in the threshold value of $(k_p)^* = k_d / y_-$, after which the system has a stable fixed point at a non-vanishing concentration of RasGTP. This result is consistent with the parameter sensitivity shown in Fig. S3c. (b) Increasing K_{pM} will result in a monotonic decrement in y_- , thus, the threshold $(k_p)^* = k_d / y_-$ will occur at a higher value than that of the base case. This is consistent with Fig. S3a. (c) Increasing K_{pM} will result in a monotonic increment in y_- , thus, the

threshold, $(k_p)^* = k_d / y_-$, will occur at a lower value than that of the base case. This is consistent with Fig. S3d.

It is now easy to study the variations of the network that will abrogate bistability in the system. We consider the following variations.

(A) Non-enzymatic Ras de-activation

If Ras deactivation was not mediated by enzymes such as RasGAPs, and we represented this process as a first order decay with a rate constant k_d . The mean field rate equation for R_T is given by,

$$\frac{d[R_T]}{dt} = \frac{k[E][R_D]}{K_M + [R_D]} + \frac{k_p[R_T][R_D]}{K_{pM} + [R_D]} - k_d[R_T] \quad (8)$$

The steady state of Eq. (8) is given by,

$$\begin{aligned} & \frac{k[E][R_D]}{K_M + [R_D]} + \frac{k_p[R_T][R_D]}{K_{pM} + [R_D]} - k_d[R_T] = 0 \\ \Rightarrow & \frac{k[E](\beta - [R_T])}{K_M + \beta - [R_T]} + \frac{k_p[R_T](\beta - [R_T])}{K_{pM} + \beta - [R_T]} - k_d[R_T] = 0 \\ \Rightarrow & k[E](\beta - x)(K_{pM} + \beta - x) + k_p x(\beta - x)(K_M + \beta - x) - k_d(K_M + \beta - x)(K_{pM} + \beta - x) = 0 \end{aligned}$$

where, $x = [R_T]$.

$$\Rightarrow a_3 x^3 + a_2 x^2 + a_1 x + a_0 = 0 \quad (9)$$

where,

$$\begin{aligned} a_3 &= k_p - k_d \\ a_2 &= k[E] + k_d(K_M + K_{pM}) + 2\beta(k_d - k_p) - K_M k_p \\ a_1 &= -K_{1M}(k[E] + k_d K_M) - \beta(2k[E] + k_d(K_M + K_{pM}) - K_M k_p) + \beta^2(k_p - k_d) \\ a_0 &= \beta k[E](\beta + K_{pM}) \end{aligned}$$

Since, $a_0 > 0$, in order to have three real positive solutions (a necessary condition to have bistability in the steady state), we should have, following Descartes rule, (i) $a_3 < 0$, (ii) $a_2 > 0$ and (iii) $a_1 < 0$.

Condition (i) gives,

$$k_d > k_p. \quad (10)$$

From (ii) we get,

$$k_d + \frac{k[E]}{K_M + K_{pM} + 2\beta} > k_p \frac{2\beta + K_M}{K_M + K_{pM} + 2\beta}, \quad (11)$$

and from (iii) we get,

$$k_d + \frac{k[E](K_{pM} + \beta)}{K_M K_{pM} + \beta(K_M + K_{pM}) + \beta^2} > k_p \frac{\beta(\beta + K_M)}{K_M K_{pM} + \beta(K_M + K_{pM}) + \beta^2} \quad (12)$$

The above conditions are not in contradiction with each other. Therefore, one could find a range of parameters where the above inequalities are satisfied and there are three real positive solutions $(\lambda_1, \lambda_2, \lambda_3)$ for x . However, if the system is bistable, the system should possess two stable real positive roots and an unstable real positive root. Now we will show that two of the above positive real roots are stable and one of them is unstable.

From Eq. (8),

$$\begin{aligned} \frac{dx}{dt} &= \frac{k[E](\beta - x)}{K_M + \beta - x} + \frac{k_p x(\beta - x)}{K_{pM} + \beta - x} - k_d x \\ &= \frac{a_3 x^3 + a_2 x^2 + a_1 x + a_0}{(K_M + \beta - x)(K_{pM} + \beta - x)} = \frac{f(x)}{g(x)} \end{aligned} \quad (13)$$

where, $f(x) = a_3 x^3 + a_2 x^2 + a_1 x + a_0$ and $g(x) = (K_M + \beta - x)(K_{pM} + \beta - x)$.

if, $x = x^* = \{\lambda_1, \lambda_2, \lambda_3\}$, is a solution of Eq.(13) then, we can perform a linear stability analysis of Eq.(13) around $x = x^*$ to find the stability of the solution.

Writing,

$x = x^* + \delta x$, Eq.(13) gives rise to the following form to linear order in δx ,

$$\frac{d(\delta x)}{dt} = \frac{\delta x}{g(x^*)} \left. \frac{df}{dx} \right|_{x=x^*} \quad (14)$$

However, $\left. \frac{df}{dx} \right|_{x=\lambda_1} = \frac{1}{a_3} (\lambda_1 - \lambda_2)(\lambda_1 - \lambda_3)$, $\left. \frac{df}{dx} \right|_{x=\lambda_2} = \frac{1}{a_3} (\lambda_2 - \lambda_1)(\lambda_2 - \lambda_3)$, and

$\left. \frac{df}{dx} \right|_{x=\lambda_3} = \frac{1}{a_3} (\lambda_3 - \lambda_1)(\lambda_3 - \lambda_2)$. Since, $g(x^*) > 0$, and, $a_3 < 0$, the necessary

condition for having three real positive solutions, with two being stable, i.e., $\left. \frac{df}{dx} \right|_{x=x^*} > 0$, and one unstable $\left(\left. \frac{df}{dx} \right|_{x=x^*} < 0 \right)$.

The steady state solutions of the system can be calculated exactly from the solutions of the cubic equation in Eq.(9) which will reveal the dependence of Ras activation on the kinetic rate constants and enzyme concentrations.

Even though this system allows for two stable positive real fixed points and an unstable positive real fixed points we show that at least one of the real positive solution corresponds to a Ras-GTP concentration larger than the total Ras concentration, β , thus this set of fixed points is clearly unphysical and the system does not show bi-stability in the physical range of parameters.

The unphysical nature of the solution will become evident if we study the dynamics of Ras-GDP, which is shown below,

$$\frac{d[R_D]}{dt} = -\frac{k[E][R_D]}{K_M + [R_D]} - \frac{k_p[R_T][R_D]}{K_{pM} + [R_D]} + k_d[R_T] \quad (15)$$

The steady state will be given by,

$$\begin{aligned} k[E]y(K_{pM} + y) + k_p y(\beta - y)(K_M + y) - k_d(\beta - y)(K_M + y)(K_{pM} + y) &= 0 \\ \Rightarrow b_3 y^3 + b_2 y^2 + b_1 y + b_0 &= 0 \end{aligned} \quad (16)$$

,where, $y = R_D$, and

$$b_3 = k_d - k_p$$

$$b_2 = k + k_d(K_M + K_{pM}) - K_M k_p + \beta(k_p - k_d)$$

$$b_1 = K_{pM}(k + k_d K_M) - \beta(k_d(K_{pM} + K_M) - K_M k_p)$$

$$b_0 = -\beta k_d K_M K_{pM}$$

In order to have three real positive roots we should have, (i) $b_3 > 0$, (ii) $b_2 < 0$ and (iii) $b_1 > 0$, since, $b_0 < 0$. If (i), (ii) and (iii) are consistent with each other, it implies,

$$K_{pM} \left[\frac{1}{1 + K_M/K_{pM}(1 - k_p/k_d)} - 1 \right] + k_p/k_d \left[\frac{1}{1 + K_M/K_{pM}(1 - k_p/k_d)} - \frac{1}{1 - k_p/k_d} \right] - \frac{K_M}{1 - k_p/k_d} > 0$$

Since, $k_d > k_p$ from condition (i), the left hand side of the above inequality is always less than zero, therefore, these conditions are not consistent with each other and Eq.(16) cannot have three positive real solutions. This is what corresponds to the unphysical negative concentrations of Ras-GDP if this system were to apparently exhibit bistability.

(B) Absence of a positive feedback

Numerically, we find that such a system does not display bistability (Fig.1D and Fig. S2E). In this case ($k_p = 0$), the dynamics of Ras activation will be given by,

$$\frac{d[R_T]}{dt} = \frac{k[E][R_D]}{K_M + [R_D]} - \frac{k_d[G][R_T]}{K_{dM} + [R_T]} \quad (17)$$

The above kinetics will produce a quadratic equation in terms of $x = [R_T]$, where, $[R_T]$ denotes the steady state concentration of Ras-GTP. Therefore, the system will not display any bistability.

(C) Catalytic Ras activation through [E] but a quadratic form of the positive feedback and a first order decay of [R_T]

This will produce an equation below,

$$\frac{d[R_T]}{dt} = \frac{k[E][R_D]}{K_M + [R_D]} + k_p[R_T][R_D] - k_d[R_T] \quad (18)$$

The steady state equation for the above dynamics gives,

$$a_3x^3 + a_2x^2 + a_1x + a_0 = 0$$

where,

$$a_3 = k_p, a_2 = k_d - (2\beta + K_M)k_p, a_1 = -k[E] + (\beta + K_M)(\beta k_p - k_d), a_0 = k[E]\beta.$$

Since, $a_3 > 0$ and $a_0 > 0$, the above cubic equation will not have three positive real solutions at the same time, therefore, the system will not display bistability.

(D) Noncatalytic Ras activation through [E] but catalytic Ras activation through positive feedback and a first order Ras deactivation

In this case, the Ras activation kinetics will be given by,

$$\frac{d[R_T]}{dt} = k[E][R_D] + \frac{k_p[R_T][R_D]}{K_{pM} + [R_D]} - k_d[R_T] \quad (19)$$

However, this will produce a quadratic equation for x at the steady state, thus, there will not be any bistability in the system.

(E) Non-catalytic Ras activation and deactivation

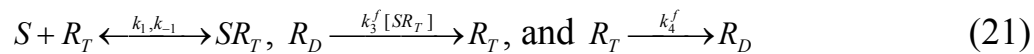
In this case the kinetics of Ras activation will appear as,

$$\frac{d[R_T]}{dt} = k[E][R_D] + k_p[R_T][R_D] - k_d[R_T] \quad (20)$$

This will give rise to a quadratic equation for x at the steady state, thus there will not be any bistability.

(F) Introduction of more molecular details in the dynamics, i.e., positive feedback mediated by an intermediate complex

Now we will explore the possibility of getting bistability in the system by going to a slightly more detailed model than Eq.(1) where, activated Ras, explicitly creates an intermediate species which mediates the positive feedback in Ras activation. We will limit ourselves to non-catalytic forms of Ras activation to emphasize our proposal that catalytic form of Ras activation and de-activation is a necessary condition to get bistability in the system. The reaction scheme for this model is given by,



In the above reaction scheme, S , R_D , R_T , SR_T denote, SOS, Ras-GDP, Ras-GTP and the complex SOS-Ras-GTP (Ras-GTP bound to SOS's allosteric site), respectively. There are two conservation laws arising from the conservation of total number of Ras and SOS molecules, given by,

$\alpha = [S] + [SR_T]$, and, $\beta = [R_D] + [R_T] + [SR_T]$. Therefore, the kinetics of the system can be described by two independent variables, $[S]$ and $[R_T]$. These variables follow the kinetic equations below,

$$\frac{d[S]}{dt} = -k_1[S][R_T] + k_{-1}[SR_T] \quad (22a)$$

$$\frac{d[R_T]}{dt} = (k_2^f + k_3^f[SR_T])[R_D] + k_1[S][R_T] - k_{-1}[SR_T] \quad (22b)$$

From now on, we will denote the variables, $[S]$ and $[R_T]$ by the variables, x_1 and x_2 , where, $x_1 = [S]$, $x_2 = [R_T]$, to keep the notations simple. In the steady state the left hand sides of the above equations will vanish, and Eq.(22a) will give,

$$x_1 = \frac{\alpha}{1 + k_{1D}x_2} \quad (23)$$

where, $k_{1D} = k_1/k_{-1}$.

The steady state equation for Eq.(22b) will produce,

$$(k_2^f + k_3^f(\alpha - x_1))(\beta - \alpha + x_1 - x_2) - k_4^f x_2 = 0 \quad (24)$$

First, we will study the case, $k_2^f = 0$. Using Eq. (23), we get from Eq.(24),

$$x_2(a_2x_2^2 + a_1x_2 + a_0) = 0 \quad (25)$$

where, $a_2 = k_{1D}^2(\alpha k_3^f + k_4^f)$, $a_1 = k_{1D}(\alpha^2 k_{1D} k_3^f + \alpha k_3^f(1 - \beta k_{1D}) + 2k_4^f)$ and $a_0 = k_4^f - \alpha \beta k_{1D} k_3^f$.

Therefore, in addition to the solution, $x_2 = 0$, there will be two real positive roots of Eq. (25) if, (i) $a_0 > 0$ and (ii) $a_1 < 0$, because, $a_2 > 0$.

Condition (i) gives,

$$k_4^f > \alpha \beta k_{1D} k_3^f \quad (26)$$

and, from (ii) using (i) we get,

$$k_4^f + \alpha^2 k_{1D} k_3^f + \alpha k_3^f < 0 \quad (27)$$

However, Eq.(27) gives an unphysical condition (negative rate constants), therefore, we cannot have three physical positive real roots at the same time, consequently, the system will not be bistable.

Now we study the case, when, $k_2^f \neq 0$. For this case, we get the following cubic equation in x_2 ,

$$a_3x^3 + a_2x^2 + a_1x + a_0 = 0 \quad (28)$$

where,

$$a_3 = k_{1D}^2(k_2^f + \alpha k_3^f + k_4^f)$$

$$a_2 = k_{1D}[(2 + k_{1D}(\alpha - \beta))k_2^f + (\alpha^2 k_{1D} + \alpha(1 - \beta k_{1D}))k_3^f + 2k_4^f]$$

$$a_1 = k_2^f(1 + k_{1D}(\alpha - 2\beta)) + k_4^f - \alpha\beta k_{1D}k_3^f$$

$$a_0 = -\beta k_2^f$$

Clearly, $a_3 > 0$ and $a_0 < 0$. Thus, Eq. (28) can possess three real positive solutions, if, (i) $a_2 < 0$ and (ii) $a_1 > 0$. From (i),

$$(2 + k_{1D}\alpha)k_2^f + \alpha(\alpha k_{1D} + 1)k_3^f + 2k_4^f < \alpha\beta k_{1D}k_3^f + 2\beta k_{1D}k_2^f \quad (29)$$

and from (ii),

$$k_2^f(1 + k_{1D}\alpha) + k_4^f > \alpha\beta k_{1D}k_3^f + 2\beta k_{1D}k_2^f \quad (30)$$

In order to Eq.(29) to be consistent with Eq. (30), we should have, $k_2^f(1 + k_{1D}\beta) + k_4^f + \alpha k_3^f(1 + \alpha k_{1D}) < 0$, which is clearly an unphysical condition. Therefore, this model also does not display bistability. The calculation reported above show that the minimal requirements for bistable Ras activation are: 1. Positive feedback regulation of SOS. 2. A catalytic activation of RasGDP by SOS with RasGTP bound to the allosteric site. 3. A catalytic deactivation mechanism for Ras deactivation by RasGAPs. Non-catalytic mechanisms do not lead to digital signaling). Interestingly, all of these features are biologically true for our system. As Fig. 1E shows, RasGRP activity make this bistability emerge effectively.